haematologica
Journal of the Ferrata Storti Foundation

Ex vivo correction of severe coagulation Factor VII deficiency in patient-derived 3D liver organoids

by Giacomo Roman, Knut H. Lauritzen, Sean P. Harrison, Anindita Bhattacharya, Marianne Seierstad Andresen, Marie-Christine Mowinckel, Barbora Smolkova, Carola E. Henriksson, Heidi Glosli, Nina Iversen, Bernd Thiede, Gareth J. Sullivan, Runar Almaas, Per Morten Sandset, Benedicte Stavik and Maria E. Chollet

Received: April 23, 2025.
Accepted: September 29, 2025.

Citation: Giacomo Roman, Knut H. Lauritzen, Sean P. Harrison, Anindita Bhattacharya, Marianne Seierstad Andresen, Marie-Christine Mowinckel, Barbora Smolkova, Carola E. Henriksson, Heidi Glosli, Nina Iversen, Bernd Thiede, Gareth J. Sullivan, Runar Almaas, Per Morten Sandset, Benedicte Stavik and Maria E. Chollet. Ex vivo correction of severe coagulation Factor VII deficiency in patient-derived 3D liver organoids.
Haematologica. 2025 Oct 9. doi: 10.3324/haematol.2025.288046 [Epub ahead of print]

Title

Ex vivo correction of severe coagulation Factor VII deficiency in patient-derived 3D liver organoids

Authors:

Giacomo Roman[1,2,3], Knut H. Lauritzen[1,2,3], Sean P. Harrison[4], Anindita Bhattacharya[1,2,3], Marianne Seierstad Andresen[2,3], Marie-Christine Mowinckel[2,3], Barbora Smolkova[4], Carola E. Henriksson[1,5], Heidi Glosli[4,6], Nina Iversen[7], Bernd Thiede[8], Gareth J. Sullivan[4,9], Runar Almaas[1,4], Per Morten Sandset[1,2,3], Benedicte Stavik[2,3], Maria E. Chollet[1,2,3]

Affiliations

[1] Institute of Clinical Medicine, University of Oslo, Oslo, Norway

[2] Department of Haematology, Oslo University Hospital, Oslo, Norway

[3] Research Institute of Internal Medicine, Oslo University Hospital, Oslo, Norway

[4] Department of Paediatric Research, Oslo University Hospital, Oslo, Norway

[5] Department of Medical Biochemistry, Oslo University Hospital, Oslo, Norway

[6] Centre for Rare Disorders, Oslo University Hospital, Oslo, Norway

[7] Department of Medical Genetics, Oslo University Hospital, Oslo, Norway

[8] Department of Biosciences, University of Oslo, Oslo, Norway

[9] School of Medicine, University of St Andrews, St Andrews, UK

Corresponding author

Maria E. Chollet; MD, PhD

m.e.c.dugarte@ous-research.no

+47 23 07 21 84

Author contributions

GR performed experiments, analyzed the data and wrote the manuscript. B Stavik, MEC, MSA, MCM, AB, B Smolkova and SPH participated in performing the experiments. HG recruited the patient. KHL, CEH and NI participated in the data analysis and revised the manuscript. RA contributed to the single-cell cloning experiments and revised the manuscript. BT performed the LC-MS experiments. GJS, B Stavik, PMS and MEC conceived and designed the study, participated in the data analysis and revised the manuscript. All authors approved the final version.

Conflict of interest

GJS is co-founder and CSO of Occam BioSciences Ltd. GJS and SPH are holders of the liver organoid technology used in this study (Patent WO2022101675A1).

All the other authors declare no conflicts of interest.

Fundings

This study was funded by the Norwegian Research Council (325869).

Acknowledgments

The authors would like to thank Ellen Skarpen at the Core Facility for Advanced Light Microscopy, Institute for Cancer Research, Oslo University Hospital, for assistance with the confocal microscopy.

Data-sharing statement

The data analyzed in this study are available from the corresponding author upon reasonable request.

Abstract

Coagulation factor (F) VII deficiency is the most frequent among the rare, inherited bleeding disorders and is predominantly caused by missense mutations in the *F7* gene. The disease phenotype ranges from asymptomatic cases to extremely severe hemorrhagic forms, requiring prophylactic injections with plasma-derived or recombinant FVII concentrates.

In response, we have developed an autologous cell-based approach that corrects the disease-causing mutation in patient-derived induced pluripotent stem cells (iPSCs) and generates therapeutic, three-dimensional hepatic organoids (HOs). We report the CRISPR-mediated correction of homozygous c.718G>C (p.G240R), a missense mutation associated with a severe, life-threatening bleeding phenotype. The HOs contain all liver cell types and exhibit key liver functions, including coagulation factor production. After correction, our data indicate that the patient-derived HOs secrete consistent amounts of functional FVII protein, resulting in improved thrombin generation times.

These results represent a significant milestone toward the establishment of an autologous cell-based therapy for patients with FVII- and other coagulation factor deficiencies.

Keywords

Coagulation FVII deficiency; Bleeding disorders; iPSCs; CRISPR; Liver organoids; Hepatic organoids; Autologous cell therapy

Introduction

Coagulation factor (F) VII deficiency is an autosomal recessive disease resulting from a wide spectrum of mutations in the *F7* gene, located at 13q34[1]. It is the most frequent among the rare, inherited bleeding disorders, with an estimated prevalence of about 1:300'000 to 1:500'000, although an increased prevalence is reported in countries like Norway[2]. The clinical phenotype ranges from asymptomatic to severe-to-lethal hemorrhagic forms, which are often associated with early age of presentation[3]. Although the correlation between the clinical phenotype and the residual FVII coagulation activity (FVII:C) is poor, a relatively small increase in activity can alleviate symptoms[1,4,5]. The current treatment for FVII deficiency relies on protein replacement with frequent and highly expensive bolus injections of FVII concentrates, either recombinant or plasma derived. Because FVII has a short half-life (less than 3 hours), patients with severe clinical phenotypes require very frequent, prophylactic injections and recurrent blood sampling for monitoring of treatment. In addition, the patients are also at risk of developing rare adverse events, such as inhibitors, i.e. antibodies neutralizing the exogenous FVII[2,5].

The main variants responsible for inherited FVII deficiency are missense mutations, which account for about 78% of the total alterations in the *F7* gene[6]. We have previously reported a homozygous missense mutation in exon 8, the guanine (G) to cytosine (C) substitution at position 718 (c.718G>C, NM_000131.4; hg38 chr13: g.113117509G>C), in two Norwegian patients with residual FVII:C <1.0 IU/dL and spontaneous, intracranial hemorrhages[2]. This single-nucleotide change leads to the amino acid substitution of arginine for glycine at position 240 (p.G240R), resulting in impaired secretion and activity of FVII *in vitro*[2], explaining the severe phenotype observed in patients.

By modulating the signaling pathways that regulate human hepatogenesis, induced pluripotent stem cells (iPSCs) can be successfully differentiated into functional hepatocytes[7,8]. We have recently reported how iPSCs can be differentiated into advanced three-dimensional hepatic organoids (HOs), which closely recapitulate the structural and functional complexity of the human liver[9]. The HOs are composed of both parenchymal (hepatocytes and cholangiocytes) and non-parenchymal cell types (hepatic stellate cells, Kupffer cells and liver sinusoidal endothelial cells). They show advanced competency in synthesizing and secreting coagulation factors, such as FVII, and coagulation inhibitors, such as antithrombin, and we have demonstrated that HOs can secrete human liver proteins into the circulation following transplantation/engraftment in mice[9].

In this study, we corrected the FVII mutation p.G240R in patient-derived iPSCs using clustered regularly interspaced short palindromic repeats (CRISPR) and CRISPR-associated

protein 9 (Cas9) technology and then differentiated both patient and gene-corrected iPSCs into functional HOs. We demonstrate that both production and secretion of functional FVII protein were restored in the corrected patient-derived HOs. This study represents a significant advancement in the development of an autologous cell-based therapy for severe FVII deficiency, which is potentially applicable to other inherited deficiencies of coagulation factors.

Methods

The study was approved by the Norwegian regional committees for medical and health research ethics (REK 2018/777) and the data protection officer at Oslo University Hospital (PVO #18/20935), and was conducted in accordance with the Helsinki Declaration.

The extended methods are present in the supplementary information (Supplementary information).

Generation and culturing of patient-derived iPSCs

Peripheral blood mononuclear cells (PBMCs) were reprogrammed to iPSCs using the CytoTune-iPS 2.0 Sendai Reprogramming Kit (Thermo Fisher Scientific; Massachusetts, USA).

Tri-lineage assessment of pluripotency

The iPSCs were directed to the definitive endoderm using the protocol developed by Mathapati et al., 2016[10] and Harrison et al., 2023[9], to mesoderm using the protocol from Lian et al., 2013[11] and to ectoderm employing the method described by Chambers et al., 2009[12] and Maroof et al., 2013[13].

CRISPR gene editing

The gene editing experiments were performed by nucleofection (Neon transfection system, Thermo Fisher Scientific) of ribonucleoprotein (RNP) complexes, assembled following IDT's recommendations (IDT; Newark, New Jersey, USA).

Droplet digital PCR (ddPCR)

The ddPCR was performed using customized NHEJ and HDR Genome Edit Detection Assays on a QX200 System and analyzed using QX Manager Software, v2.1 (Bio-Rad; California, USA).

Immunofluorescence and microscopy

Immunofluorescence analyses were performed following Harrison et al., 2023[9] for the HOs and the Cell Signaling protocol (Massachusetts, USA) for the iPSCs, and using ECHO Revolve RVL-100-M, Zeiss LSM 880 Airyscan FAST and Andor Dragonfly Spinning Disk confocal microscopes.

Sanger sequencing and whole exome sequencing (WES)

Sanger sequencing, WES analyses at 30x (Clinical Research Exome) and 100x coverage and downstream bioinformatic analysis were performed by Eurofins Genomics (Ebersberg, Germany).

Hepatic organoid differentiation

Hepatic organoids (HOs) were generated using the protocol developed by Harrison et al.[9]. On day 19, the HOs were incubated with serum-free L-15 medium, supplemented with 5 µg/mL Vitamin K_1. Both HOs and the cell supernatant were collected on day 21 for downstream analyses, after 2 days in serum-free conditions.

Protein determination and activity assay

FVII protein levels and activity were analyzed by U-PLEX Human Factor VII (Mesoscale Diagnostic; Maryland, USA) and BIOPHEN FVII assay (Aniara; Ohio, USA), respectively. Factor X, albumin and α-1 Antitrypsin (A1AT) antigens were measured by enzyme-linked immunosorbent assay (ELISA). Thrombin generation was assessed by calibrated automated thrombogram (CAT) (Diagnostica Stago; Asnières sur Seine, France), by mixing HO supernatant with FVII-deficient plasma. Total protein was quantified with Pierce BCA Protein Assay Kits (VWR; Radnor, Pennsylvania, USA).

Liquid chromatography-mass spectrometry (LC-MS) analysis

LC-MS was performed on SDS-PAGE bands using a timsTOF Pro spectrometer (Bruker Daltonik; Bremen, Germany). Data analysis was performed using Scaffold v5.1.2 (Proteome Software Inc.; Oregon, USA).

Statistical analyses

The statistical analyses and graphs were performed with GraphPad Prism 10.2.0. The data were generated from three independent experiments consisting of two biological replicates for the HOs and one for the PHs and are expressed as mean and standard deviation. The normal distribution was assessed by Shapiro-Wilk test. For the comparison among two groups the statistical significance was determined by unpaired Student's t-test. A probability value of $p<0.05$ was considered statistically significant.

Results

Generation and characterization of patient-derived iPSCs

The primary PBMCs isolated from the peripheral blood of the FVII deficient patient were reprogrammed to iPSCs using Sendai virus and, on appearance of iPSC colonies, clones were picked based on correct morphology. After passaging of clones for 10 to 12 passages we demonstrated the complete clearance of any residual Sendai reprogramming factor, compared to PBMCs 3 days after transduction (Figure 1A). After 20 passages, genetic stability was investigated by karyotyping, revealing no evidence of aneuploidy or rearrangements (Figure 1B). To corroborate this further and profile the patient-derived iPSCs genetic background, whole exome sequencing was performed. When mapped against the GRCh38 reference assembly and filtered according to allele frequency (AF) ≥ 0.01 and read depth (DP) ≥ 20, no relevant short variants, such as single nucleotide variants (SNVs) or small insertions/deletions (InDels), were detected in the *F7* gene, but only the c.718G>C missense SNV corresponding to the severe p.G240R mutation (Figure 1C).

Next, pluripotency was examined in the confirmed Sendai-free iPSCs, first by assessing the pluripotency markers OCT4, NANOG and SOX2 by immunofluorescence, and expression of all markers was detected (Figure 2A and B). We then assessed tri-lineage potential by differentiating the iPSCs into the three germ layers. We assessed endoderm potential by differentiating to definitive endoderm, producing iPSCs that were $FOXA2^+/SOX17^+$ double-positive, during both 3 µM and 4 µM CHIR99021 conditions (Figure 2C). Further gene expression analyses demonstrated that all the conditions exhibited the upregulation of both *FOXA2* and *SOX17* endoderm-specific markers (Figure 2D). When differentiated to the ectoderm lineage, the resulting neuroepithelium was $NESTIN^+/SOX2^+/PAX6^+$ positive (Figure

2E), a combination of markers specific for neural progenitor cells[14]. Using RT-qPCR we showed a 47-fold upregulation of *PAX6* expression (Figure 2F). For mesoderm, we differentiated iPSCs to cardiomyocytes, and after 2 weeks we observed spontaneously contracting cardiomyocytes, from 24 and $36 \cdot 10^3$ iPSCs/cm^2 under both 8 µM and 10 µM CHIR99021 (Supplementary video file 1). We further validated by assessing the cardiac-specific marker Cardiac Troponin I (cTnI) which we observed (Figure 2G), as well as significant upregulation of Troponin T2 (*TNNT2*), used as a cardiac-specific mRNA marker for all the different differentiation conditions (Figure 2H). We observed the *TNNT2* upregulation up to 40-fold, in cardiomyocytes from $36 \cdot 10^3$ iPSCs/cm^2 under 8 µM CHIR99021 (Figure 2H).

Gene correction of *F7* c.718G>C missense mutation and iPSC cloning

To gene edit c.718G>C, six different gRNAs were designed *in silico* (Supplementary figure 1A). Following nucleofection, the intracellular presence of the CRISPR RNPs was verified by fluorescent microscopy (Supplementary figure 1B). The on-target cutting activity of each gRNA was evaluated post nucleofection using the droplet digital polymerase chain reaction (ddPCR). The analysis of non-homologous end joining (NHEJ) event by ddPCR indicated a fractional abundance, i.e. the ratio edited alleles (FAM^+/HEX^- droplets)/total alleles (FAM^+, FAM^+/HEX^+), of 41% and 48% for gRNA #2 and gRNA #5, respectively, meaning that ~50% of the population of alleles carried a NHEJ event (Supplementary figure 1C and D). The corresponding values for the negative control, consisting of CRISPR components nucleofected without gRNA, was 0% (Supplementary figure 1C and D). As a result, gRNA #5 was chosen as an ideal candidate to perform gene correction of *F7* c.718G>C in patient-derived iPSCs (Supplementary figure 2A). For the correction we leveraged homology-directed repair (HDR), we explored how efficiency was influenced under different concentrations of the HDR enhancer V2. Using ddPCR analyses we observed HDR rates ranging from 19.4% (no enhancer) up to 50.7% (1 µM V2 HDR enhancer) (Supplementary figure 2B and C). To maximize the HDR rate while minimizing the concentration of V2 HDR enhancer, we selected CRISPR HDR pools with 0.25 µM HDR enhancer. From this, single cell-derived iPSC clones were then successfully generated. A detailed monoclonality report was generated for each single cell (Supplementary figure 3) by combining the sorting data with the clonal iPSC follow-up by plate imaging. The impedance signals were analyzed to meet highly stringent quality criteria, such as optimal particle size (≥400 and ≤3'000 ohm) and low background signal noise, during both detection and dispensing. No sign of

differentiation and/or morphological abnormalities in the single cell-derived iPSC colony were identified. iPSCs that passed these criteria were then screened for HDR occurrence at the target locus by Sanger sequencing, which also functioned as an initial screen for monoclonality (Figure 3A).

Off-target analysis and Whole Exome Sequencing (WES)

We next assessed potential off-target sites predicted by Benchling (Benchling; San Francisco, California, USA) and IDT using whole exome sequencing (WES). We cross-checked with the variant calling report, generated by filtering the comparison between the original patient iPSC line carrying the c.718G>C mutation (control) against corrected iPSC clones. With AF ≥ 0.01 and DP ≥ 20, we observed no off-target effects, relevant and/or deleterious variants possibly associated with CRISPR editing (Supplementary table file 2). The WES confirmed the correction of c.718G>C was present at 100%, with 45x coverage (Figure 3B). This also further validated monoclonality of the corrected iPSC clone.

Differentiation to HOs and *in vitro* assessment of FVII production

Both patient and corrected iPSCs were differentiated into HOs (Figure 4A, B and C). To investigate FVII production in liver organoids we generated iPSC-derived HOs as described by Harrison et al.[9]. We assessed efficiency and quality of the differentiation at day 6, by assessing the expression of the hepatic marker HNF4A. Both p.G240R control and corrected HOs were positive for HNF4A (Figure 4B). On passing the QC stage the HOs were cultured until day 19 when they reached a mature state and presented with liver-like cellular complexity. At day 21 we assessed the markers HNF4A and asialoglycoprotein receptor 1 (ASGR1), a marker for mature hepatocytes[9,15], by immunofluorescence (Figure 4C). We next assessed the HOs for key hepatic attributes at the transcriptional level. Using RT-qPCR we verified the presence of hepatic markers *HNF4A* and two Cytochrome P450 (*CYP450*) enzymes, *CYP3A4* and *CYP3A7* (Figure 4D). When compared to p.G240R control HOs and primary hepatocytes (PHs), the corrected HOs showed increased transcription of *HNF4A*, of about ~2 fold ($p<0.001$). Interestingly, *CYP3A4* expression in corrected HOs was increased by ~10.1-fold ($p<0.01$) when compared to control p.G240R HOs but reduced to ~0.12-fold when compared to PHs (Figure 4D). In contrast, *CYP3A7* expression in corrected HOs was downregulated ~6.5-fold, when compared to control p.G240R HOs ($p<0.001$). We then assessed the production and secretion of two liver-specific proteins, albumin (ALB) and alpha-1-antitrypsin (A1AT) by ELISA (Figure 4E). While we detected similar amounts of

secreted ALB, A1AT secretion was decreased by ~1.79-fold in the corrected HOs, when compared to the control p.G240R HOs ($p<0.01$) (Figure 4E). We also assessed *F10* at the mRNA level and FX antigen levels (FX:Ag) (Figure 5A), where we observed no significant differences in levels after correction of the *F7* mutation.

Finally, we investigated FVII production in HOs. First, we found that *F7* transcription in the corrected HOs increased by ~1.39 fold, when compared to control p.G240R ($p<0.01$) (Figure 5B). Next, we examined intracellular FVII synthesis by quantitative U-PLEX FVII assay and immunostaining. Corrected HOs exhibited a 9-fold increase ($p<0.0001$) in the intracellular FVII levels, reaching 1.32 ± 0.32 pg/µg total protein when compared to control p.G240R HOs (0.14 ± 0.009 pg/µg total protein) (Figure 5B). Immunostaining confirmed the presence of intracellular FVII in both control p.G240R and corrected HOs (Figure 5C). Notably, while we could detect both *F7* transcript and intracellular FVII protein in the control p.G240R HOs, no FVII antigen was found in the supernatant measured by U-PLEX FVII assay. On the other hand, the corrected HOs secreted 3.97 ± 1.1 pg/µg total cellular protein, thus confirming that the gene correction successfully restored both physiological FVII synthesis and secretion (Figure 5B). We next conducted LC-MS analyses on the culture supernatants and lysates derived from two independent experiments of both control p.G240R and corrected HOs (Figure 6). After SDS-PAGE separation, we excised gel fragments between 40-60 kDa, corresponding to the expected molecular weight of FVII (~52 kDa) (Supplementary figure 9). FVII peptides were identified in the corrected HO supernatants, with sequence coverage of 18% and 15%, respectively (Figure 6A). In contrast, no FVII peptides were detected in the control p.G240R HO supernatants. As a positive reference, PH supernatant showed detectable FVII peptides with 8% sequence coverage (Figure 6D). In the lysate fraction, FVII peptides were found in both corrected HO samples (13% and 15% coverage) (Figure 6C), and in one of the two p.G240R control HO lysates (5% coverage) (Figure 6B).

To address the functional activity of the FVII produced, we investigated the ability of secreted FVII to activate FX, in presence of thromboplastin. We detected an absolute FVII chromogenic activity of 0.053 ± 0.012% of plasma calibrator in the corrected HOs (Figure 7A). In this context, corrected HOs secreted 0.41 ± 0.15 ng/mL of FVII:Ag, while control p.G240R HOs remained negative (ND) and PHs (positive control) secreted 1.32 ± 0.12 ng/mL (Figure 7A). As positive references, PHs and pooled normal plasma (PNP) reached 0.93 ± 0.19 and 121.2% of plasma calibrator, respectively. Additionally, we included HOs derived from a healthy, unedited and wild type (WT) iPSC line (AG27)[9], which showed an absolute chromogenic activity of 0.086% of plasma calibrator and served as a more suitable iPSC-derived HO control system (Figure 7A). The corresponding specific FVII activity, i.e. the relative functional output of the secreted protein, of the corrected HOs was 1.38 ± 0.32

mIU/ng FVII. In contrast, control p.G240R HOs and L-15 medium control remained negative (ND) (Figure 7B). The AG27 WT HOs showed a specific activity of 0.825 ± 0.01 mIU/ng, while PHs and PNP reached 7.06 ± 0.89 mIU/ng and 7.66 mIU/ng, respectively (Figure 7B). To further expand on the functional characterization of the rescued FVII, we also performed a thrombin generation assay to assess the overall hemostatic potential of the secreted FVII in a dynamic, plasma-based system (Figure 7C and D). Results showed that the lag time was reduced from 16.22 ± 0.8 to 12.05 ± 0.49 ($p<0.0001$) in the corrected HOs compared to the p.G240R control, when triggered with the standard 5 pM tissue factor (TF) (Figure 7C). To further challenge the sensitivity and dynamics of the assay, we repeated the test using 1 pM of TF trigger. The results confirmed our previous findings, with a prolonged lag time of 20.67 ± 2 in the p.G240R control versus 16.07 ± 1.3 in the corrected HOs ($p<0.001$) (Figure 7D).

Discussion

Here we report the successful *ex vivo* correction of a severe FVII deficiency, providing *in vitro* proof-of-concept evidence for the potential development of a cell-based therapy approach using autologous HOs for treatment of these patients. As demonstrated by pioneering studies on Hemophilia A and B[16–20], different CRISPR-Cas9 editing strategies have been used to correct mutations in *F8* and *F9* genes, and produce gene-corrected patient-derived iPSCs for further therapeutic purposes, but to date this approach has not been used to restore FVII function. Currently, over 271 different pathogenic variants within the *F7* gene have been reported by the European Association for Hemophilia and Allied Disorders (EAHAD) database[21], with the majority being missense mutations. For this reason, we present the rescue of the debilitating missense c.718G>C variant, encoding a p.G240R substitution in the catalytic domain of FVII[2,22–24], where more than half of the mutations are found[2,21], which causes a very severe clinical phenotype. In addition, another variant, the c.718G>A missense mutation, encodes the same amino acid substitution (p.G240R) and has been described in three different studies, two of which report a homozygous c.718G>A ,that causes fatal, intracranial hemorrhaging[22–24]. The patients with homozygous c.718G>A had undetectable FVII:Ag and FVII:C <1.0 IU/dL. Thus, the chosen mutation has shown consistency in phenotype severity across affected individuals and emerges as an ideal candidate for such therapy.

Efficacy and safety are central considerations in the advancement of CRISPR- and cell-based therapies[25]. In this study, we show that it is possible to streamline the pipeline for generating autologous cell products for FVII deficiency without mitigating efficacy or safety.

Firstly, we demonstrate robust reprogramming of somatic cells (PBMCs) into iPSCs, without causing any observable genome instability or the introduction of mutations in protein coding genes. Secondly, we demonstrate efficient and safe gene correction, with no CRISPR-related off-target effects or relevant, deleterious modifications identified. The transient delivery of the Cas9 nuclease/gRNA as an RNP complex, ensures that the Cas9 is active immediately upon entering the cell and rapidly cleared from the cell, maximizing on-target activity and minimizing off-target effects[26,27]. In contrast, plasmid-based methods require extended time for the CRISPR components to be synthesized and be active on-target. For this reason, they typically associate with Cas9 persistence over time (>72 hours), which significantly increases the risks of off-target effects and leads to unpredictable variability, due to Cas9 and gRNA expression levels[26,28]. Although newer CRISPR tools such as prime editing and base editing are emerging and have been utilized for gene editing both *in vitro* and *in vivo* (mouse) [29–31], the nuclease-based CRISPR-Cas9 technology has recently received FDA approval for the treatment of sickle cell disease and β-thalassemia, demonstrating its safety and potential for clinical use[32]. Thirdly, as the exposure to CRISPR-Cas9 may result in mixed populations of cells harboring different editing outcomes, the establishment of stable, monoclonal iPSC lines with a defined genotype is particularly important from a safety point of view. Using an impedance-based system that allows for the single-cell detection and gentle dispensing (≤2 psi) of the iPSCs, we demonstrate high-throughput and rapid single-cell cloning of edited cells without having to rely on manual colony picking, limiting dilution, or fluorescence-activated cell sorting that are less efficient, labor-intensive and more obtrusive[33–35]. The resulting monoclonality also provides a key advantage for genome assessment, as any variant or editing-associated effect would be uniformly represented across the entire cell population, enhancing detection sensitivity. For this reason, the WES coverage and filtering criteria employed in this study provided confident detection of coding variants, offering reliable detection of potential off-target effects within protein-coding genes. However, we recognize the importance of expanding this analysis to whole-genome sequencing (WGS) to achieve a more comprehensive, base-pair resolution profile, including non-coding or regulatory regions not fully captured by WES. Such in-depth analysis would further strengthen the safety assessment of genome-edited cell lines, particularly in the context of future clinical translation.

We have reported that p.G240R control and CRISPR-corrected iPSCs undergo HO differentiation with similar efficiency and yield, with both expressing key liver markers and secreting liver-specific proteins. Although ALB and FX secretion levels were comparable, we observed increased *HNF4A* and *CYP3A4* expression, as well as decreased *CYP3A7* transcription and A1AT secretion in the corrected HOs. While these findings may suggest

features of hepatic zonation or mature phenotype and FVII has been associated with coagulation-independent effects in the liver[9,36,37], they remain to be further investigated. Most notably, the gene correction strategy successfully rescued the FVII deficient phenotype in patient-derived HOs *ex vivo*. Consistent with the previous evidence[2], we demonstrated by RT-qPCR, U-PLEX and LC-MS analyses that the c.718G>C (p.G240R) variant does not abolish transcription and translation of FVII, but associates with severely impaired protein secretion. In contrast, the correction enabled the secretion of biologically functional FVII. Although the corrected HOs showed a substantial increase in FVII secretion compared to the p.G240R control, the corresponding increase in activity was comparatively modest, particularly when compared to the PH and PNP positive controls. The reason for this is not known, but it aligns with previous observations on the broader challenge of detecting the activity of vitamin K–dependent proteins *in vitro*, which might be affected by rapid protein degradation, dilution in the supernatant volume, as well as several other factors, such as culture medium and incubation time[19,38,39]. Whether the modest FVII activity measured in the HO-derived supernatant is explained by the instability and/or activation of the FVII protein in the serum-free cell medium with consequent functional degradation, complex formation, or other forms of inhibition[19,38,39] remains to be thoroughly investigated.

In this study, PHs were included as a positive control rather than as a benchmark comparator for therapeutic performance. Unlike HOs, which recapitulate the multicellular architecture and complexity of the liver, PHs represent a highly purified monolayer of terminally differentiated primary hepatocytes, cultured at high density in low-volume conditions for only a few days. These fundamental differences in cell composition, density, and media volume limited the direct comparisons in terms of absolute secretion or functional output. To address this and accurately characterize functional output, we calculated the specific activity (mIU/ng) by normalizing measured FVII:C to FVII:Ag levels and confirmed that the protein secreted by corrected HOs was functionally active. To expand on this further, the thrombin generation assays provided additional functional insight, demonstrating a more substantial correction of the overall coagulation profile. This assay provides a comprehensive view of the coagulation kinetic by measuring thrombin generation over time in FVII-deficient plasma supplemented with HO-derived supernatant. The marked reduction in lag time suggested that the restored FVII secretion translated into biologically functional activity. Notably, these results also indicate that the rescued FVII protein underwent the post-translation modifications that are required for proper secretion and biological function[40–43]. However, the clinical relevance of this rescue remains to be further investigated. The HO production can be exponentially expanded offering the potential to generate therapeutically relevant quantities for transplantation[9]. In this perspective, although the capacity of HOs to

engraft and sustain long-term secretion of human liver proteins *in vivo* has already been demonstrated by Harrison et al.[9], the next essential objective of this study will be to assess therapeutic efficacy in a disease-relevant *in vivo* model.

Conclusion

In conclusion, we demonstrate the first *in vitro* correction of severe FVII deficiency, using patient-derived, CRISPR-corrected liver organoids. Our study presents a proof of principle in the development of a novel cell therapy for FVII deficiency, with potential applicability across the spectrum of inherited coagulation factor deficiencies.

References

1. Chollet ME, Andersen E, Skarpen E, et al. Factor VII deficiency: Unveiling the cellular and molecular mechanisms underlying three model alterations of the enzyme catalytic domain. Biochim Biophys Acta Mol Basis Dis. 2018;1864(3):660-667.

2. Andersen E, Chollet ME, Sletten M, et al. Molecular Characterization of Two Homozygous Factor VII Variants Associated with Intracranial Bleeding. Thromb Haemost. 2021;121(12):1588-1598.

3. Mariani G, Herrmann FH, Dolce A, et al. Clinical phenotypes and factor VII genotype in congenital factor VII deficiency. Thromb Haemost. 2005;93(3):481-487.

4. Napolitano M, Siragusa S, Mariani G. Factor VII deficiency: Clinical phenotype, genotype and therapy. J Clin Med. 2017;6(4):38.

5. Robinson KS. An overview of inherited factor VII deficiency. Transfus Apher Sci. 2019;58(5):569-571.

6. Bernardi F, Dolce A, Pinotti M, et al. Major differences in bleeding symptoms between factor VII deficiency and hemophilia B. J Thromb Haemost. 2009;7(5):774-779.

7. Si-Tayeb K, Noto FK, Nagaoka M, et al. Highly efficient generation of human hepatocyte-like cells from induced pluripotent stem cells. Hepatology. 2010;51(1):297-305.

8. Sullivan GJ, Hay DC, Park IH, et al. Generation of functional human hepatic endoderm from human induced pluripotent stem cells. Hepatology. 2010;51(1):329-335.

9. Harrison SP, Siller R, Tanaka Y, et al. Scalable production of tissue-like vascularized liver organoids from human PSCs. Exp Mol Med. 2023;55(9):2005-2024.

10. Mathapati S, Siller R, Impellizzeri AAR, et al. Small-molecule-directed hepatocyte-like cell differentiation of human pluripotent stem cells. Curr Protoc Stem Cell Biol. 2016;2016(1):1G.6.1-1G.6.18.

11. Lian X, Zhang J, Azarin SM, et al. Directed cardiomyocyte differentiation from human pluripotent stem cells by modulating Wnt/β-catenin signaling under fully defined conditions. Nat Protoc. 2013;8(1):162-175.

12. Chambers SM, Fasano CA, Papapetrou EP, Tomishima M, Sadelain M, Studer L. Highly efficient neural conversion of human ES and iPS cells by dual inhibition of SMAD signaling. Nat Biotechnol. 2009;27(3):275-280.

13. Maroof AM, Keros S, Tyson JA, et al. Directed differentiation and functional maturation of cortical interneurons from human embryonic stem cells. Cell Stem Cell. 2013;12(5):559-572.

14. Zhang M, Ngo J, Pirozzi F, Sun YP, Wynshaw-Boris A. Highly efficient methods to obtain homogeneous dorsal neural progenitor cells from human and mouse embryonic stem cells and induced pluripotent stem cells. Stem Cell Res Ther. 2018;9(1):1-13.

15. Peters DT, Henderson CA, Warren CR, et al. Asialoglycoprotein receptor 1 is a specific cell-surface marker for isolating hepatocytes derived from human pluripotent stem cells. Development. 2016;143(9):1475-1481.

16. Son JS, Park CY, Lee G, et al. Therapeutic correction of hemophilia A using 2D endothelial cells and multicellular 3D organoids derived from CRISPR/Cas9-engineered patient iPSCs. Biomaterials. 2022;283:121429.

17. Lyu C, Shen J, Wang R, et al. Targeted genome engineering in human induced pluripotent stem cells from patients with hemophilia B using the CRISPR-Cas9 system. Stem Cell Res Ther. 2018;9(1):92.

18. Ramaswamy S, Tonnu N, Menon T, et al. Autologous and Heterologous Cell Therapy for Hemophilia B toward Functional Restoration of Factor IX. Cell Rep. 2018;23(5):1565-1580.

19. Luce E, Steichen C, Allouche M, et al. In vitro recovery of FIX clotting activity as a marker of highly functional hepatocytes in a hemophilia B iPSC model. Hepatology. 2022;75(4):866-880.

20. Park CY, Kim DH, Son JS, et al. Functional Correction of Large Factor VIII Gene Chromosomal Inversions in Hemophilia A Patient-Derived iPSCs Using CRISPR-Cas9. Cell Stem Cell. 2015;17(2):213-220.

21. Giansily-Blaizot M, Rallapalli PM, Perkins SJ, et al. The EAHAD blood coagulation factor VII variant database. Hum Mutat. 2020;41(7):1209-1219.

22. Landau D, Rosenberg N, Zivelin A, Staretz-Chacham O, Kapelushnik J. Familial factor VII deficiency with foetal and neonatal fatal cerebral haemorrhage associated with homozygosis to Gly180Arg mutation. Haemophilia. 2009;15(3):774-778.

23. Giansily-Blaizot M, Aguilar-Martinez P, Biron-Andreani C, et al. Analysis of the genotypes and phenotypes of 37 unrelated patients with inherited factor VII

deficiency. Eur J Hum Genet. 2001;9(2):105-112.

24. Kuperman AA, Barg AA, Fruchtman Y, et al. Primary prophylaxis for children with severe congenital factor VII deficiency - Clinical and laboratory assessment. Blood Cells Mol Dis. 2017;67:86-90.

25. Pacesa M, Pelea O, Jinek M. Past, present, and future of CRISPR genome editing technologies. Cell. 2024;187(5):1076-1100.

26. DeWitt MA, Corn JE, Carroll D. Genome editing via delivery of Cas9 ribonucleoprotein. Methods. 2017;121-122:9-15.

27. Vakulskas CA, Dever DP, Rettig GR, et al. A high-fidelity Cas9 mutant delivered as a ribonucleoprotein complex enables efficient gene editing in human hematopoietic stem and progenitor cells. Nat Med. 2018;24(8):1216-1224.

28. Kim S, Kim D, Cho SW, Kim J, Kim J-S. Highly efficient RNA-guided genome editing in human cells via delivery of purified Cas9 ribonucleoproteins. Genome Res. 2014;24(6):1012-1019.

29. Chen PJ, Liu DR. Prime editing for precise and highly versatile genome manipulation. Nat Rev Genet. 2023;24(3):161-177.

30. Li C, Georgakopoulou A, Newby GA, et al. In vivo HSC prime editing rescues sickle cell disease in a mouse model. Blood. 2023;141(17):2085-2099.

31. Zeng J, Wu Y, Ren C, et al. Therapeutic base editing of human hematopoietic stem cells. Nat Med. 2020;26(4):535-541.

32. Parums DV. Editorial: First Regulatory Approvals for CRISPRCas9 Therapeutic Gene Editing for Sickle Cell Disease and Transfusion-Dependent b-Thalassemia. Med Sci Monit. 2024;30:e944204.

33. Tristan CA, Hong H, Jethmalani Y, et al. Efficient and safe single-cell cloning of human pluripotent stem cells using the CEPT cocktail. Nat Protoc. 2023;18(1):58-80.

34. Chen YH, Pruett-Miller SM. Improving single-cell cloning workflow for gene editing in human pluripotent stem cells. Stem Cell Res. 2018;31:186-192.

35. Singh AM. An Efficient Protocol for Single-Cell Cloning Human Pluripotent Stem Cells. Front Cell Dev Biol. 2019;7:11.

36. Zhang Y, Jiang Q, Liang X, et al. Coagulation Factor VII Fine-tunes Hepatic Steatosis by Blocking AKT-CD36-Mediated Fatty Acid Uptake. Diabetes. 2024;73(5):682-700.

37. Zabulica M, Srinivasan RC, Vosough M, et al. Guide to the Assessment of Mature Liver Gene Expression in Stem Cell-Derived Hepatocytes. Stem Cells Dev. 2019;28(14):907-919.

38. Lengler J, Coulibaly S, Gruber B, et al. Development of an In Vitro Biopotency Assay for an AAV8 Hemophilia B Gene Therapy Vector Suitable for Clinical Product Release. Mol Ther Methods Clin Dev. 2020;17:581-588.

39. Nederlof A, Kitchen S, Meijer P, et al. Performance of factor IX extended half-life product measurements in external quality control assessment programs. J Thromb Haemost. 2020;18(8):1874-1883.

40. Bolt G, Steenstrup TD, Kristensen C. All post-translational modifications except propeptide cleavage are required for optimal secretion of coagulation factor VII. Thromb Haemost. 2007;98(5):988-997.

41. Bolt G, Kristensen C, Steenstrup TD. More than one intracellular processing bottleneck delays the secretion of coagulation factor VII. Thromb Haemost. 2008;100(2):204-210.

42. Clarke BJ, Sridhara S. Incomplete gamma carboxylation of human coagulation factor VII: Differential effects on tissue factor binding and enzymatic activity. Br J Haematol 1996;93(2):445-450.

43. Wang H, Wang L, Li S, Dong N, Wu Q. N-Glycan-calnexin interactions in human factor VII secretion and deficiency. Int J Biochem Cell Biol. 2019;113:67-74.

44. Mathijssen NCJ, Masereeuw R, Holme PA, et al. Increased volume of distribution for recombinant activated factor VII and longer plasma-derived factor VII half-life may explain their long lasting prophylactic effect. Thromb Res. 2013;132(2):256-262.

Figure legends

Figure 1. Genetic characterization of patient-derived iPSCs (c.718G>C, p.G240R). (A) Quantitative RT-qPCR to assess Sendai clearance, using 18S endogenous control. PBMCs after 3 days from transduction were used as a positive control. Results are expressed as mean ± SD (n = 3). “Not detected” (ND) indicates undetermined Ct values. (B) KaryoStat+ Assay Report. The whole genome view displays all somatic and sex chromosomes in one frame with high level copy number. The smooth signal plot (right, y-axis) is the smoothing of the log2 ratios which depict the signal intensities of probes on the microarray. A value of 2 represents a normal copy number state (CN = 2). A value of 3 represents chromosomal gain (CN = 3). A value of 1 represents a chromosomal loss (CN = 1). The pink, green and yellow colors indicate the raw signal for each individual chromosome probe, while the blue signal represents the normalized probe signal. (C) Integrative Genomics Viewer (IGV; igv.org) view from the Illumina WES INVIEW Human Exome 100x analysis. Sequencing reads are presented in grey, the GRCh38/hg38 reference sequence is located at the top, under the chromosomal coordinates. c.718G>C mismatch is presented in blue.

Figure 2. Functional characterization of iPSC pluripotency by tri-lineage differentiation assay. (A) Brightfield image of the selected iPSC clone (500 µm scale bar). (B) Immunofluorescence analysis on the selected iPSC clone for pluripotency markers (from left) SOX2 (green), OCT4 (red), and NANOG (cyan) (100 µm scale bar). Zeiss LSM 880 Airyscan FAST confocal microscope. (C, left) Immunofluorescence analysis on the iPSC-derived definitive endoderm for FOXA2 (green) and SOX2 (red), cultured with B27 (-) + 4 µM CHIR. (C, right) FOXA2 (green) and SOX17 (red), for the iPSC-derived definitive endoderm cultured with B27 (-) + 3 µM CHIR (100 µm scale bar). (D) Quantitative RT-qPCR analysis of definitive endoderm-associated markers *FOXA2* and *SOX17*, using 18S endogenous control. iPSCs (p22) were used as a control. Results are expressed as mean ± SD (n = 3). Statistical significance was determined by unpaired t-test, with *** $p<0.001$ and ** $p<0.01$. (E) Immunofluorescence analysis on the iPSC-derived neuroepithelium, for PAX6 (green), SOX2 (red) and NESTIN (cyan) (100 µm scale bar). (F) Quantitative RT-qPCR analysis of *PAX6* expression, in the iPSC-derived neuroepithelium. Results are expressed as mean ± SD (n = 3), * $p<0.05$ with unpaired t-test. (G) Immunofluorescence analysis on the iPSC-derived cardiomyocytes, for cTnI (green) (100 µm scale bar). (H) Quantitative RT-qPCR analysis of *TNNT2* expression. Results are expressed as mean ± SD (n = 3), *** $p<0.001$ with unpaired t-test.

Figure 3. Genetic characterization of a gene-corrected, single cell-derived iPSC clone. (A) Sanger sequencing view of gRNA #5/ssODN donor-targeted locus, at exon 8 of F7. c.718G>C, p.G240R control (top) and a homozygous, corrected iPSC clone (bottom). Generated with SnapGene® Viewer 7.2.1. (B) Integrative Genomics Viewer (IGV; igv.org) view from the Illumina Clinical Research Exome - CRE V4 analysis. Sequencing reads are presented in grey, the GRCh38/hg38 reference sequence is located at the top, under the chromosomal coordinates. c.718G>C, p.G240R control (top) and a homozygous, corrected iPSC clone (bottom).

Figure 4. Generation and characterization of p.G240R control and corrected HOs. (A) Brightfield images of p.G240R control (left) and corrected HOs (right), at day 0 and day 19 of the differentiation (500 µm scale bar). ECHO Revolve RVL-100-M. (B) Immunofluorescence analysis for HNF4A marker on p.G240R control (left) and corrected HOs (right), at day 6 (500 µm and 100 µm scale bar). ECHO Revolve RVL-100-M. (C) Immunofluorescence analysis for ASGR1 and HNF4A markers on p.G240R control (left) and corrected HOs (right), at day 19 (100 µm scale bar). Andor Dragonfly Spinning Disk confocal microscope. (D) Quantitative RT-qPCR analysis of *HNF4A*, and two enzymes of the *CYP450* enzyme family, *CYP3A4* and *CYP3A7* (from left to right), using 18S endogenous control. Results are normalized to PHs and expressed as mean ± SD. Statistical significance was determined by unpaired t-test, with * $p<0.05$ and **** $p<0.0001$. (E) ALB and A1AT quantification by ELISA assay. Results were normalized to the total cellular protein and adjusted to the culture volume, and expressed as mean ± SD. Statistical significance was determined by unpaired t-test, with ** $p<0.01$.

Figure 5. FX and FVII analysis. (A, left) Quantitative RT-qPCR analysis of *F10* expression, using 18S endogenous control. Results are normalized to PHs and expressed as mean ± SD. Statistical significance was determined by unpaired t-test. (A, right) FX antigen quantification by ELISA assay. Results were normalized to the total cellular protein and adjusted to the culture volume, and expressed as mean ± SD. Statistical significance was determined by unpaired t-test. (B, left) Quantitative RT-qPCR analysis of *F7* expression, using 18S endogenous control. Results are normalized to PHs and expressed as mean ± SD. Statistical significance was determined by unpaired t-test, with ** $p<0.01$. (B, middle) Intracellular FVII antigen quantification by U-PLEX assay. Results were normalized to the total cellular protein and expressed as mean ± SD. Statistical significance was determined

by unpaired t-test, **** p<0.0001. (B, right) Secreted FVII antigen quantification by U-PLEX assay. Results were normalized to the total cellular protein and adjusted to the culture volume, and expressed as mean ± SD. “Not detected” (ND) indicates values below the assay detection limit. (C) Immunofluorescence analysis for FVII and HNF4A markers on p.G240R control (left) and corrected HOs (right), at day 19 (100 µm scale bar). Andor Dragonfly Spinning Disk confocal microscope.

Figure 6. LC-MS analysis. (A) Sequence coverage from the LC-MS analysis of the corrected HO supernatants (40-60 kDa samples, positive for FVII), (B) the control HO (p.G240R) lysate (40-60 kDa), (C) the corrected HO lysates (40-60 kDa) and (D) the PH supernatant (40-60 kDa). Identified matching peptide sequences are highlighted in yellow and bold.

Figure 7. FVII activity and total coagulation analyses. (A, left) BIOPHEN FVII analysis to determine absolute FVII chromogenic activity in cell culture supernatant. Results were expressed as % of plasma assay calibrator and as mean ± SD. Statistical significance was determined by unpaired t-test, **** p<0.0001. (A, right, up) Quantification of FVII absolute secretion by U-PLEX assay. Results were expressed in ng/mL, as mean ± SD. (B) Specific FVII chromogenic activity calculated by dividing the activity in mIU by the corresponding antigen level in ng. The conversion from % activity to IU (FVII:C) was based on Mathijssen et al.[44]. “Not detected” (ND) indicates values below the assay detection limit. (C) Thrombin generation assay using 5 pM TF trigger. (D) Thrombin generation assay using 1 pM TF trigger. Results were expressed in minutes, as mean ± SD. Statistical significance (for samples with n= 6) and determined by unpaired t-test, with *** p<0.001 and **** p<0.0001.

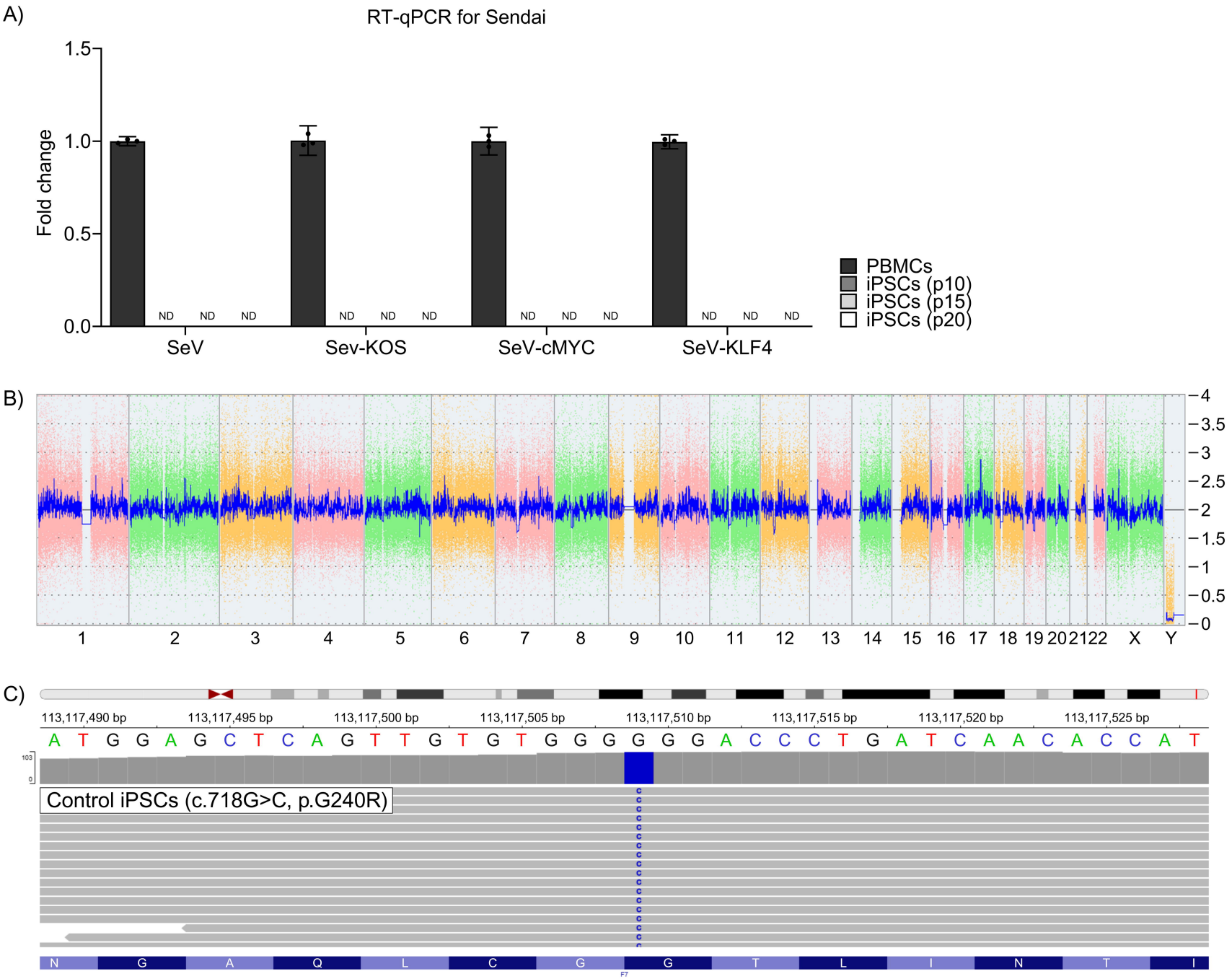
A)
RT-qPCR for Sendai
Fold change
1.5
1.0
0.5
0.0
ND
SeV
Sev-KOS
SeV-cMYC
SeV-KLF4
PBMCs
iPSCs (p10)
iPSCs (p15)
iPSCs (p20)
B)
1 2 3 4 5 6 7 8 9 10 11 12 13 14 15 16 17 18 19 20 21 22 X Y
4
3.5
3
2.5
2
1.5
1
0.5
0
C)
113,117,490 bp
113,117,495 bp
113,117,500 bp
113,117,505 bp
113,117,510 bp
113,117,515 bp
113,117,520 bp
113,117,525 bp
A T G G A G C T C A G T T G T G T G G G G G G A C C C T G A T C A A C A C C A T
Control iPSCs (c.718G>C, p.G240R)
N G A Q L C G G T L I N T I

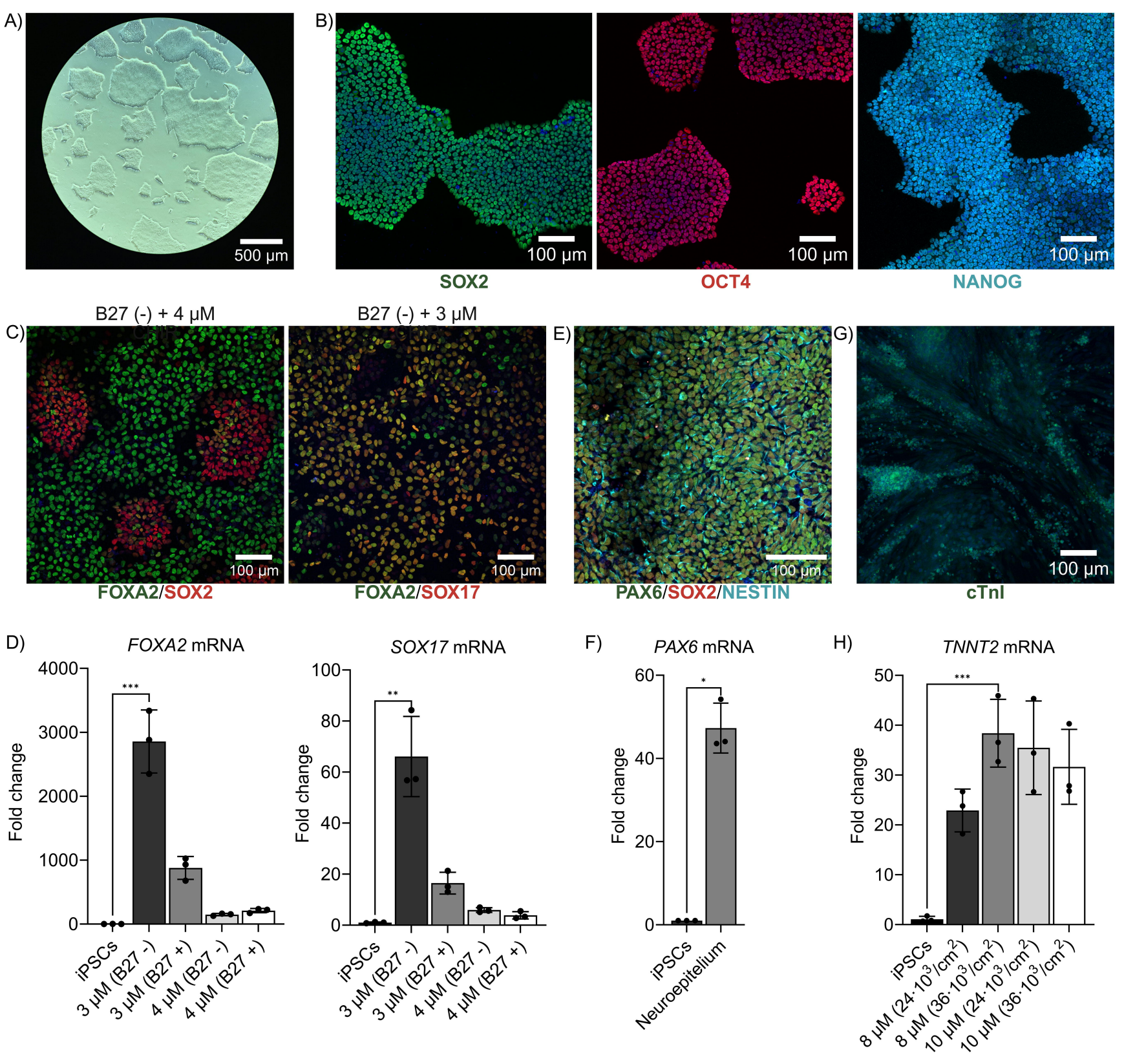
A)
500 µm
B)
100 µm
100 µm
100 µm
SOX2
OCT4
NANOG
B27 (-) + 4 µM
B27 (-) + 3 µM
C)
100 µm
100 µm
FOXA2/SOX2
FOXA2/SOX17
E)
100 µm
PAX6/SOX2/NESTIN
G)
100 µm
cTnI
D)
FOXA2 mRNA
Fold change
4000
3000
2000
1000
0
***
iPSCs
3 µM (B27 -)
3 µM (B27 +)
4 µM (B27 -)
4 µM (B27 +)
SOX17 mRNA
Fold change
100
80
60
40
20
0
**
iPSCs
3 µM (B27 -)
3 µM (B27 +)
4 µM (B27 -)
4 µM (B27 +)
F)
PAX6 mRNA
Fold change
60
40
20
0
*
iPSCs
Neuroepitelium
H)
TNNT2 mRNA
Fold change
50
40
30
20
10
0
***
iPSCs
8 µM (24·10³/cm²)
8 µM (36·10³/cm²)
10 µM (24·10³/cm²)
10 µM (36·10³/cm²)

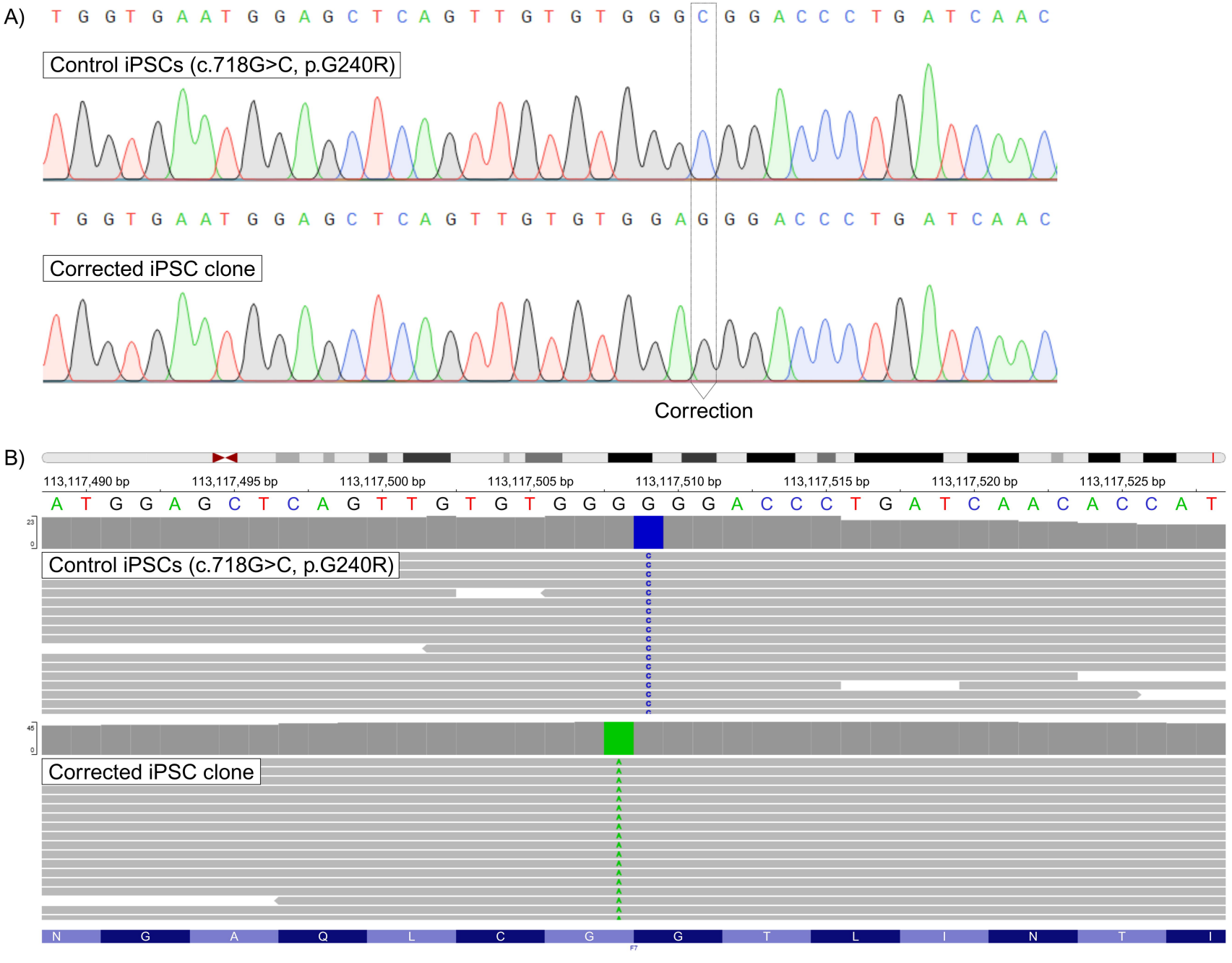
A)
T G G T G A A T G G A G C T C A G T T G T G T G G G C G G A C C C T G A T C A A C
Control iPSCs (c.718G>C, p.G240R)
T G G T G A A T G G A G C T C A G T T G T G T G G A G G G A C C C T G A T C A A C
Corrected iPSC clone
Correction
B)
113,117,490 bp
113,117,495 bp
113,117,500 bp
113,117,505 bp
113,117,510 bp
113,117,515 bp
113,117,520 bp
113,117,525 bp
A T G G A G C T C A G T T G T G T G G G G G G A C C C T G A T C A A C A C C A T
Control iPSCs (c.718G>C, p.G240R)
Corrected iPSC clone
N G A Q L C G G T L I N T I

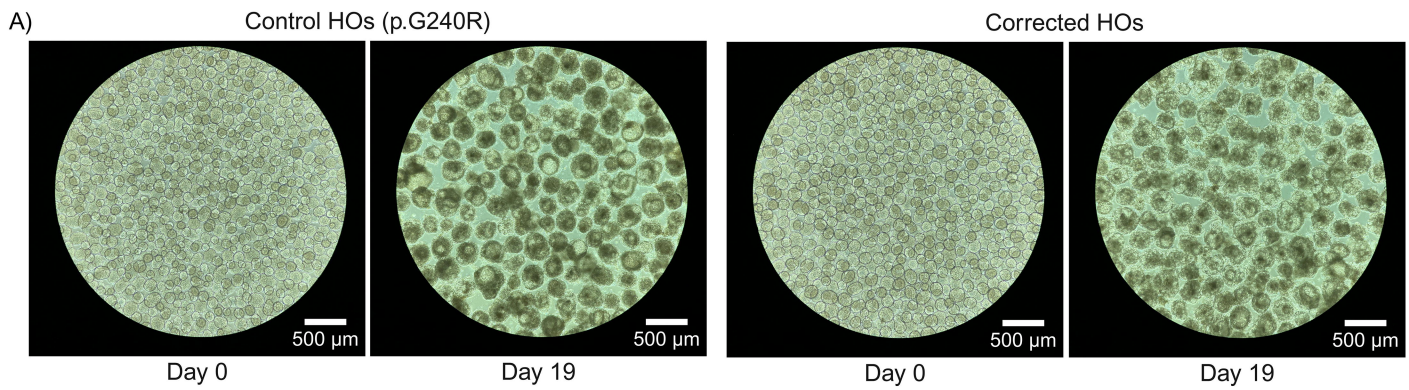
A)
Control HOs (p.G240R)
Corrected HOs
500 µm
Day 0
Day 19

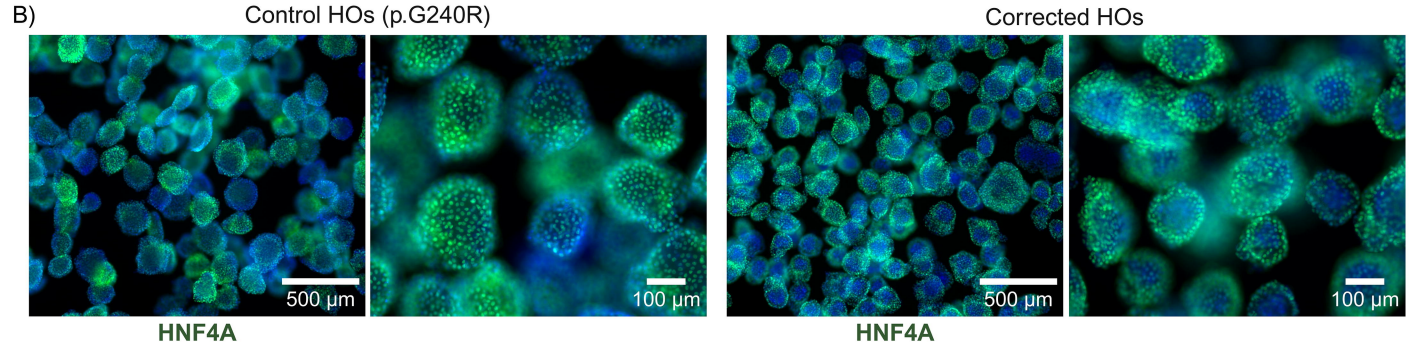
B)
Control HOs (p.G240R)
Corrected HOs
500 µm
100 µm
HNF4A

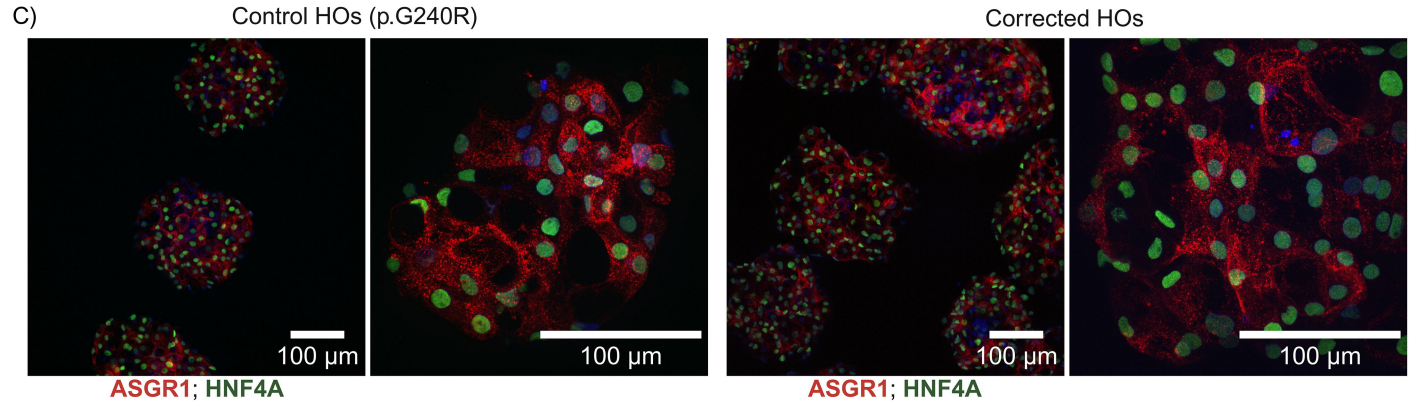
C)
Control HOs (p.G240R)
Corrected HOs
100 µm
ASGR1; HNF4A

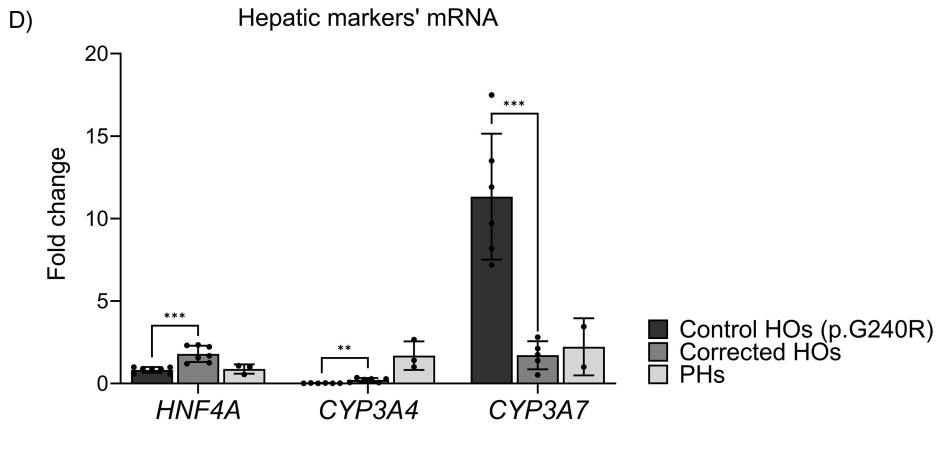
D)
Hepatic markers' mRNA
Fold change
HNF4A
CYP3A4
CYP3A7
Control HOs (p.G240R)
Corrected HOs
PHs

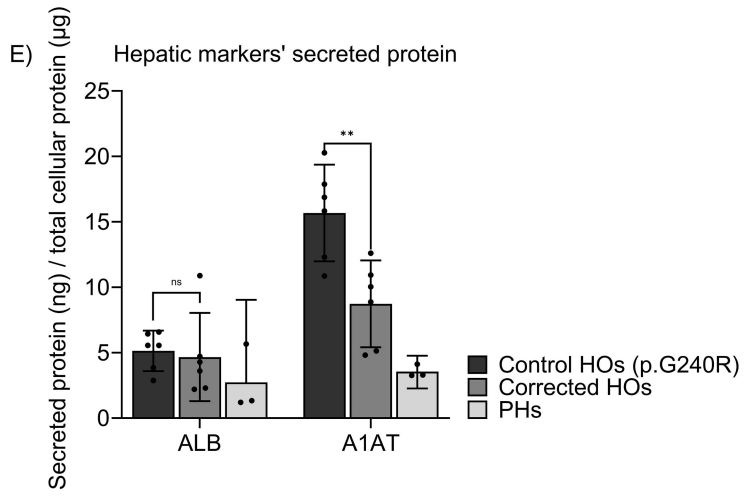
E)
Hepatic markers' secreted protein
Secreted protein (ng) / total cellular protein (µg)
ALB
A1AT
Control HOs (p.G240R)
Corrected HOs
PHs

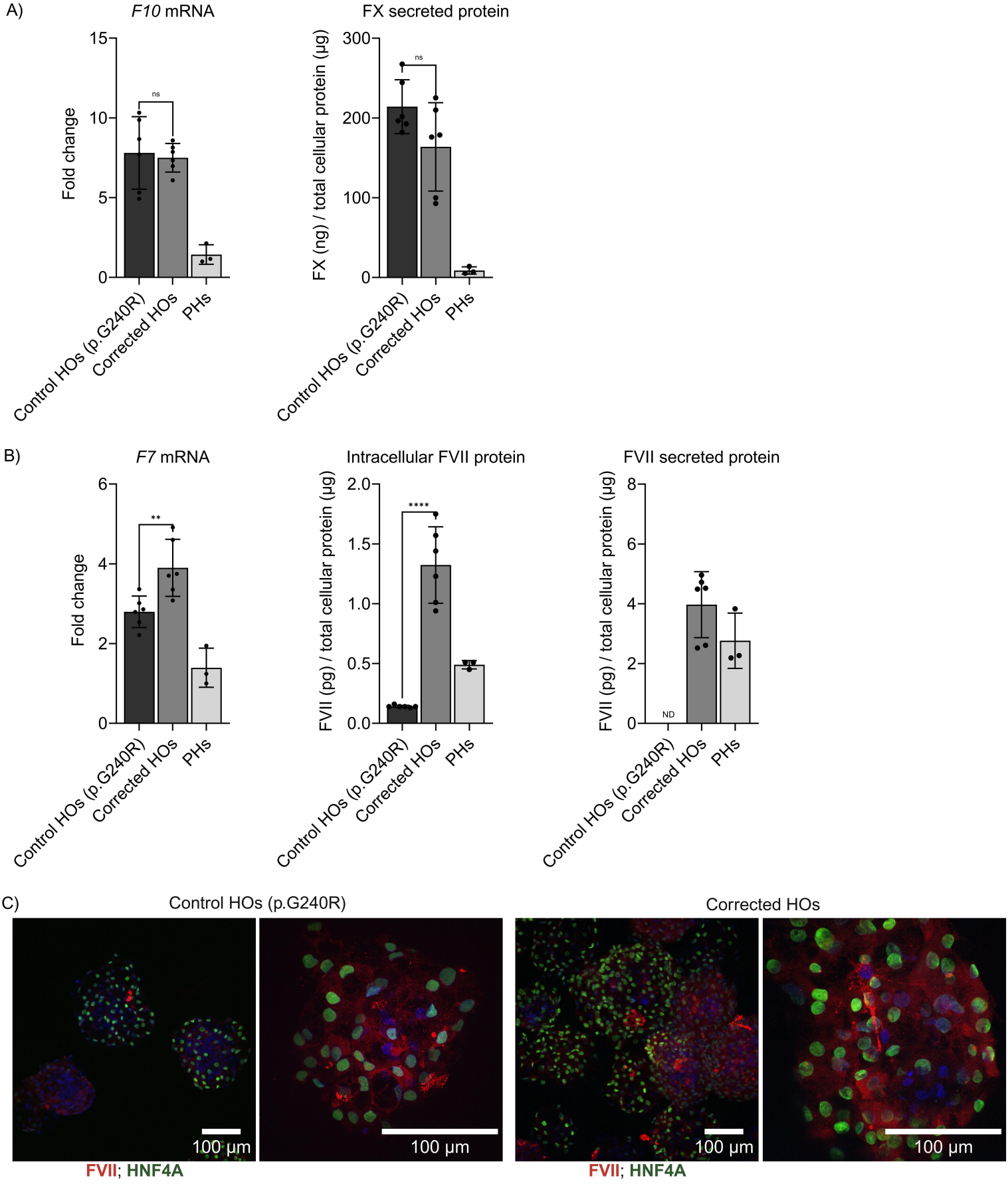
A)
F10 mRNA
Fold change
15
10
5
0
ns
Control HOs (p.G240R)
Corrected HOs
PHs
FX secreted protein
FX (ng) / total cellular protein (µg)
300
200
100
0
ns
Control HOs (p.G240R)
Corrected HOs
PHs
B)
F7 mRNA
Fold change
6
4
2
0
**
Control HOs (p.G240R)
Corrected HOs
PHs
Intracellular FVII protein
FVII (pg) / total cellular protein (µg)
2.0
1.5
1.0
0.5
0.0
****
Control HOs (p.G240R)
Corrected HOs
PHs
FVII secreted protein
FVII (pg) / total cellular protein (µg)
8
6
4
2
0
ND
Control HOs (p.G240R)
Corrected HOs
PHs
C)
Control HOs (p.G240R)
Corrected HOs
100 µm
100 µm
100 µm
100 µm
FVII; HNF4A
FVII; HNF4A

A) Corrected HOs (Supernatant)

6 exclusive unique peptides, 7 exclusive unique spectra, 9 total spectra, 83/466 amino acids (18% coverage)

5 exclusive unique peptides, 6 exclusive unique spectra, 6 total spectra, 72/466 amino acids (15% coverage)

B) Control HOs (p.G240R) (Lysate)

2 exclusive unique peptides, 2 exclusive unique spectra, 2 total spectra, 22/466 amino acids (5% coverage)

C) Corrected HOs (Lysate)

4 exclusive unique peptides, 4 exclusive unique spectra, 4 total spectra, 59/466 amino acids (13% coverage)

5 exclusive unique peptides, 5 exclusive unique spectra, 6 total spectra, 72/466 amino acids (15% coverage)

D) PHs (Supernatant)

2 exclusive unique peptides, 2 exclusive unique spectra, 2 total spectra, 36/466 amino acids (8% coverage)

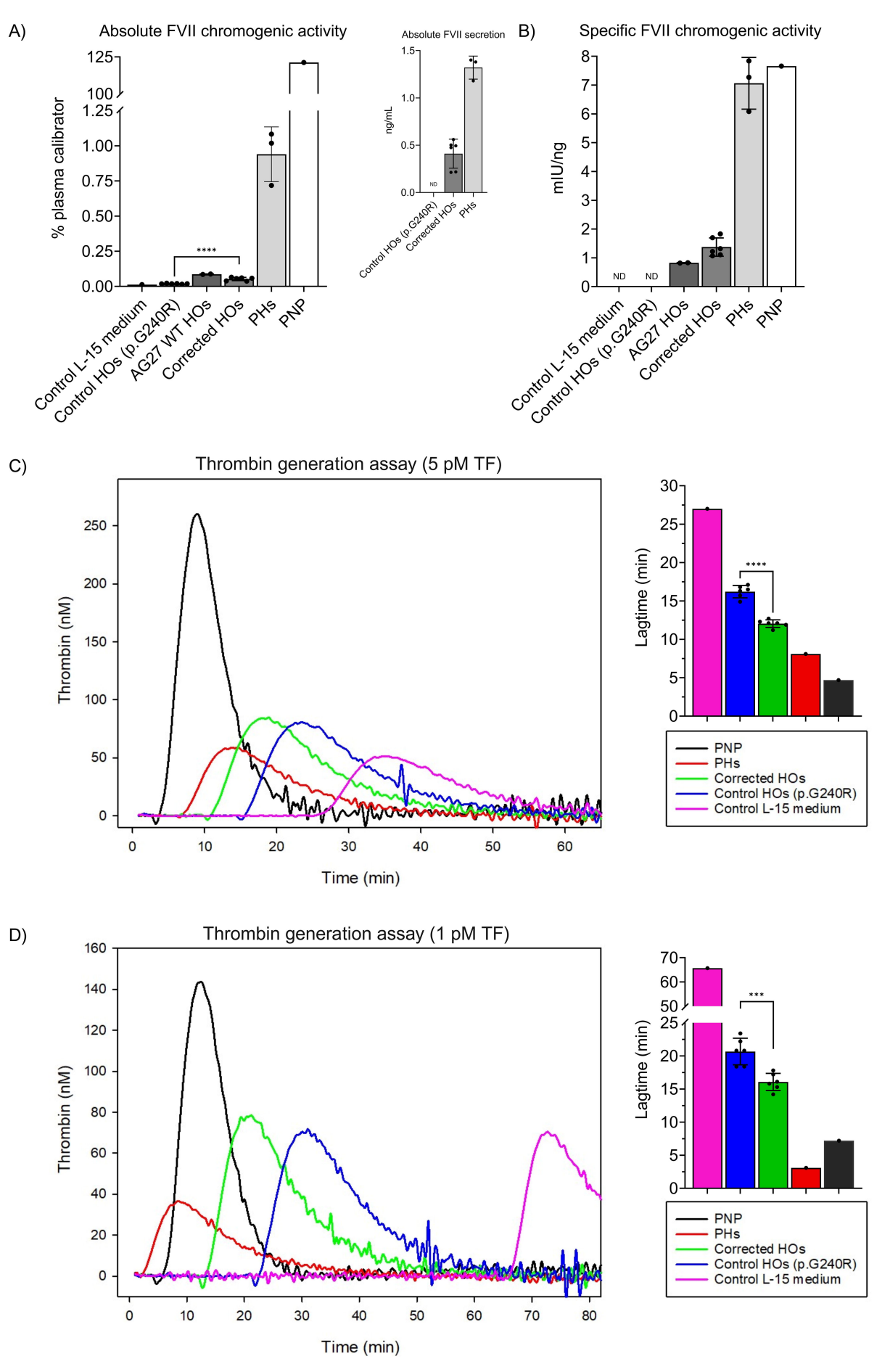
A)
Absolute FVII chromogenic activity
% plasma calibrator
125
100
1.25
1.00
0.75
0.50
0.25
0.00
****
Absolute FVII secretion
ng/mL
1.5
1.0
0.5
0.0
ND
Control HOs (p.G240R)
Corrected HOs
PHs
Control L-15 medium
Control HOs (p.G240R)
AG27 WT HOs
Corrected HOs
PHs
PNP
B)
Specific FVII chromogenic activity
mIU/ng
8
7
6
5
4
3
2
1
0
ND
ND
Control L-15 medium
Control HOs (p.G240R)
AG27 HOs
Corrected HOs
PHs
PNP
C)
Thrombin generation assay (5 pM TF)
Thrombin (nM)
250
200
150
100
50
0
0
10
20
30
40
50
60
Time (min)
Lagtime (min)
30
25
20
15
10
5
0
****
PNP
PHs
Corrected HOs
Control HOs (p.G240R)
Control L-15 medium
D)
Thrombin generation assay (1 pM TF)
Thrombin (nM)
160
140
120
100
80
60
40
20
0
0
10
20
30
40
50
60
70
80
Time (min)
Lagtime (min)
70
60
50
25
20
15
10
5
0
***
PNP
PHs
Corrected HOs
Control HOs (p.G240R)
Control L-15 medium

Supplementary information

Ex vivo correction of severe coagulation Factor VII deficiency in patient-derived 3D liver organoids

This document includes:

- Supplementary figures and figure legends
- Supplementary table file legends
- Supplementary video file legend
- Supplementary materials and methods
- References

Supplementary figures

Supplementary figure 1

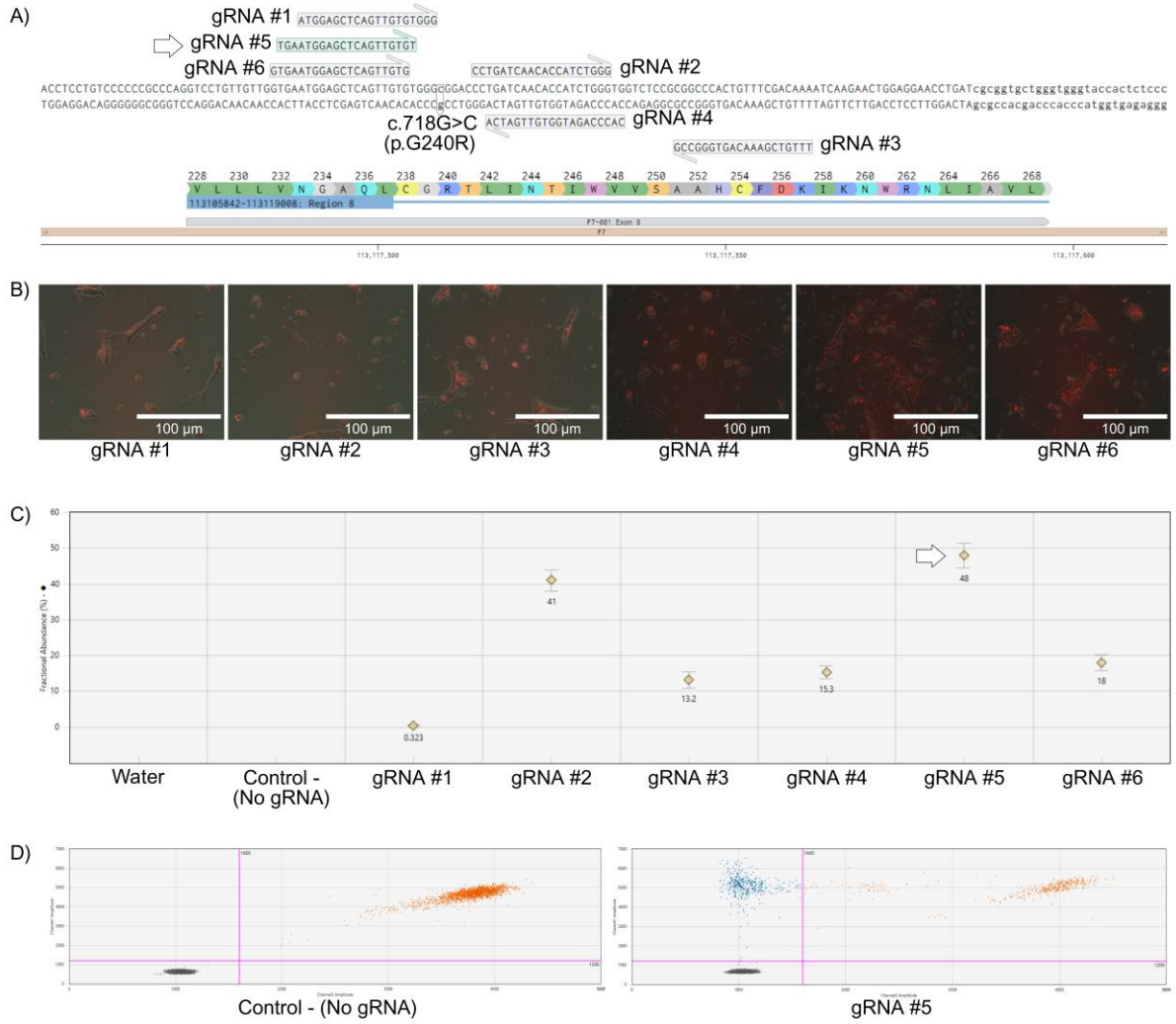

Supplementary figure 1. gRNA design and screening. Selected gRNA candidate (gRNA #5) is indicated with an arrow. (A) Summary of the gRNA panel. Created with Benchling. (B) Merge of brightfield and ATTO 550 (red) fluorescence, for each nucleofected RNP complex. (100 µm scale bar). (C, D) ddPCR NHEJ Genome Edit Detection Assays. On-target efficiency is displayed as fractional abundance (%), calculated as NHEJ edited alleles/(WT + NHEJ edited alleles), i.e. edited alleles/total alleles. (E) 2D drop-off amplitude view of c.718G>C, p.G240R control (left) and gRNA #5 (right). HEX amplitude on x-axis, FAM amplitude on y-axis. FAM^{+}/HEX^{+} cluster is represented in orange, FAM^{+}/HEX^{-} cluster in blue.

Supplementary figure 2

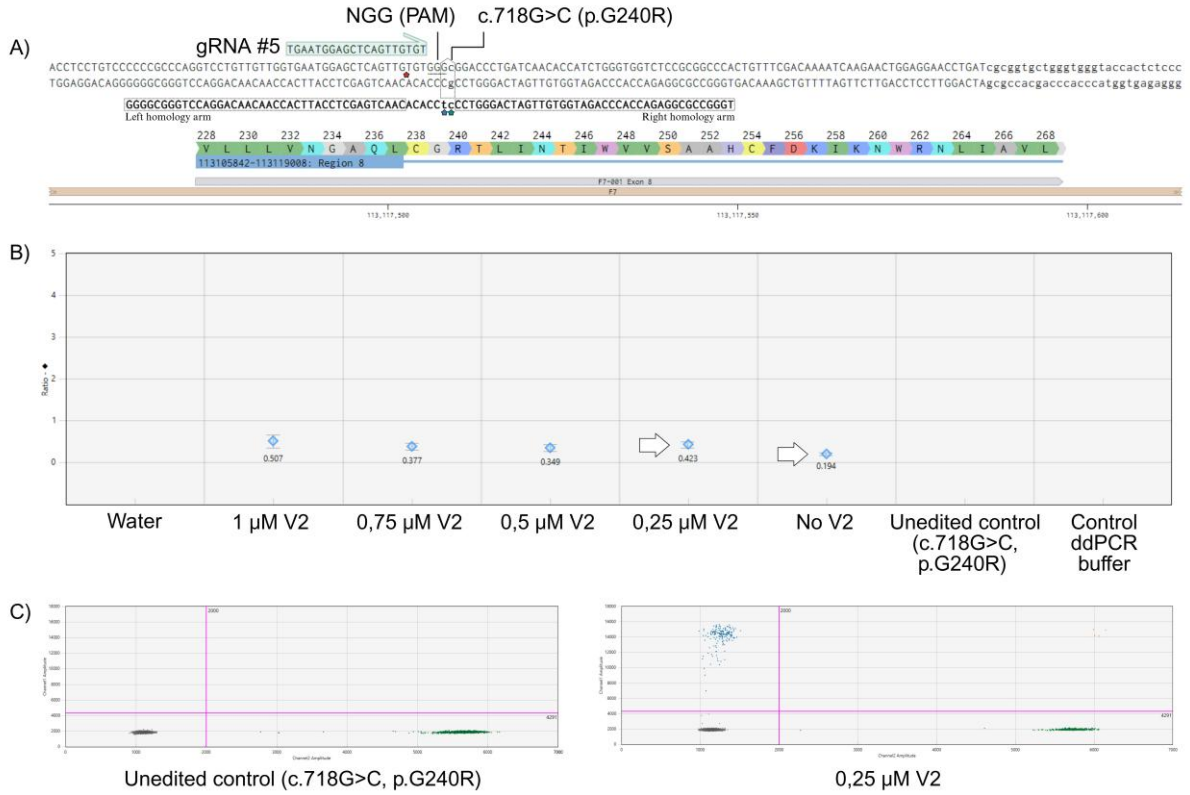

Supplementary figure 2. HDR experiment design and analysis. (A) Summary of the HDR design (gRNA #5/ssODN donor). The cut site is indicated by a red star, while the synonymous PAM-altering mutation and the therapeutic correction by a blue and green star, respectively (top). (B) ddPCR Homology Directed Repair Genome Edit Detection (HDR GED) assay for interrogating the HDR outcome at different concentration of Alt-R HDR Enhancer V2. The ratio provided is the number of HDR alleles/total number of alleles, and the percentage of total HDR efficiency can be obtained as ratio*100. Selected HDR pools are indicated by an arrow. (C) 2D amplitude view of HDR GED assay for c.718G>C, p.G240R control (left) and 0.25 µM Alt-R HDR Enhancer V2 (right). HEX amplitude on x-axis, FAM amplitude on y-axis. FAM^{+}/HEX^{+} cluster is represented in orange, FAM^{+}/HEX^{-} cluster in blue, $FAM^{-}HEX^{+}$ cluster in green.

Supplementary figure 3

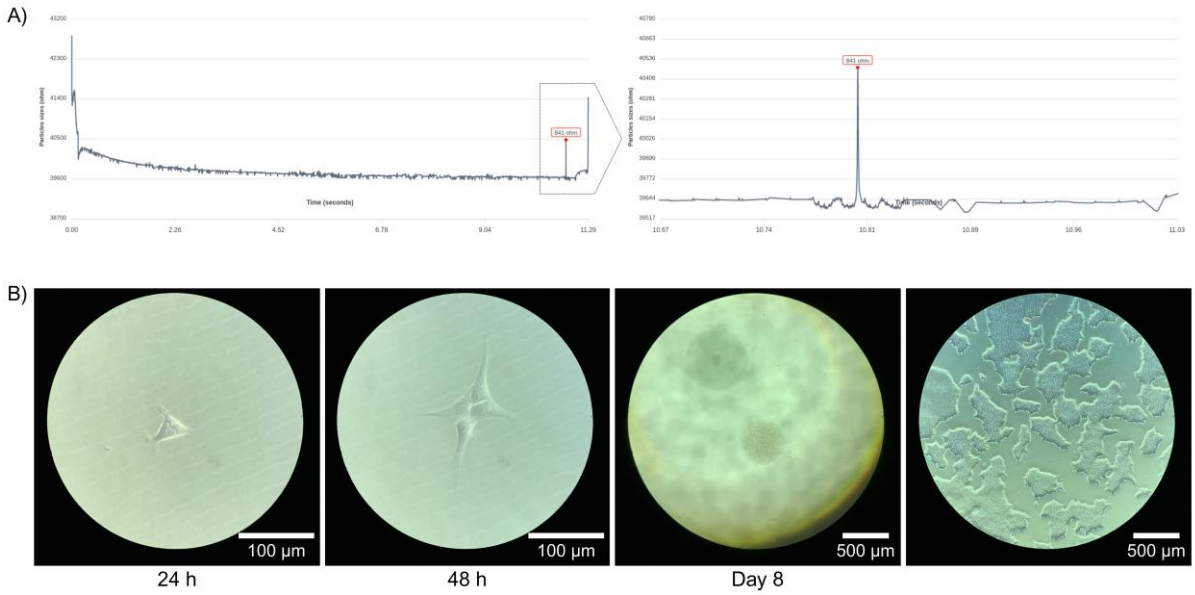

Supplementary figure 3. Single cell cloning of gene-edited iPSCs. (A) Whole view of the impedance-based monoclonality report from SEED DispenCell-S3 (left) and magnification of the single cell-induced signal record (right). Time (second) on x-axis and particle size (ohm) on y-axis. (B) Example of a growing single cell-derived, iPSC clone, after 24 hours from dispensing (left), 48 hours (middle) and 8 days (right). (100 µm and 500 µm scale bar).

Supplementary figure 4

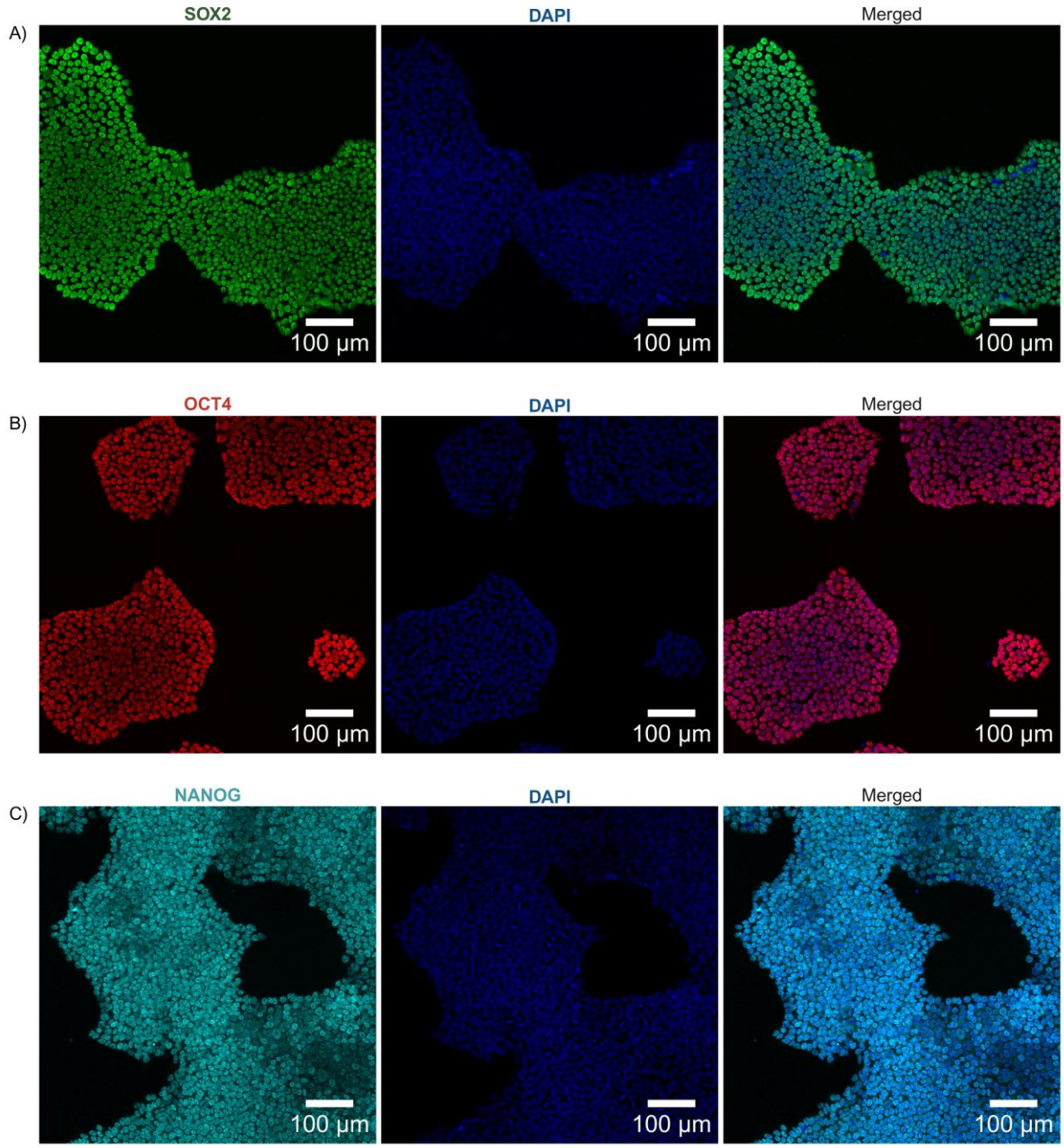

Supplementary figure 4. Single channels of the immunofluorescence analyses for the key pluripotency markers. (A) SOX2 (left, green), DAPI (middle, blue) and merged (right) (100 µm scale bar). (B) OCT4 (left, red), DAPI (middle, blue) and merged (right) (100 µm scale bar). (C) NANOG (left, cyan), DAPI (middle, blue) and merged (right) (100 µm scale bar).

Supplementary figure 5

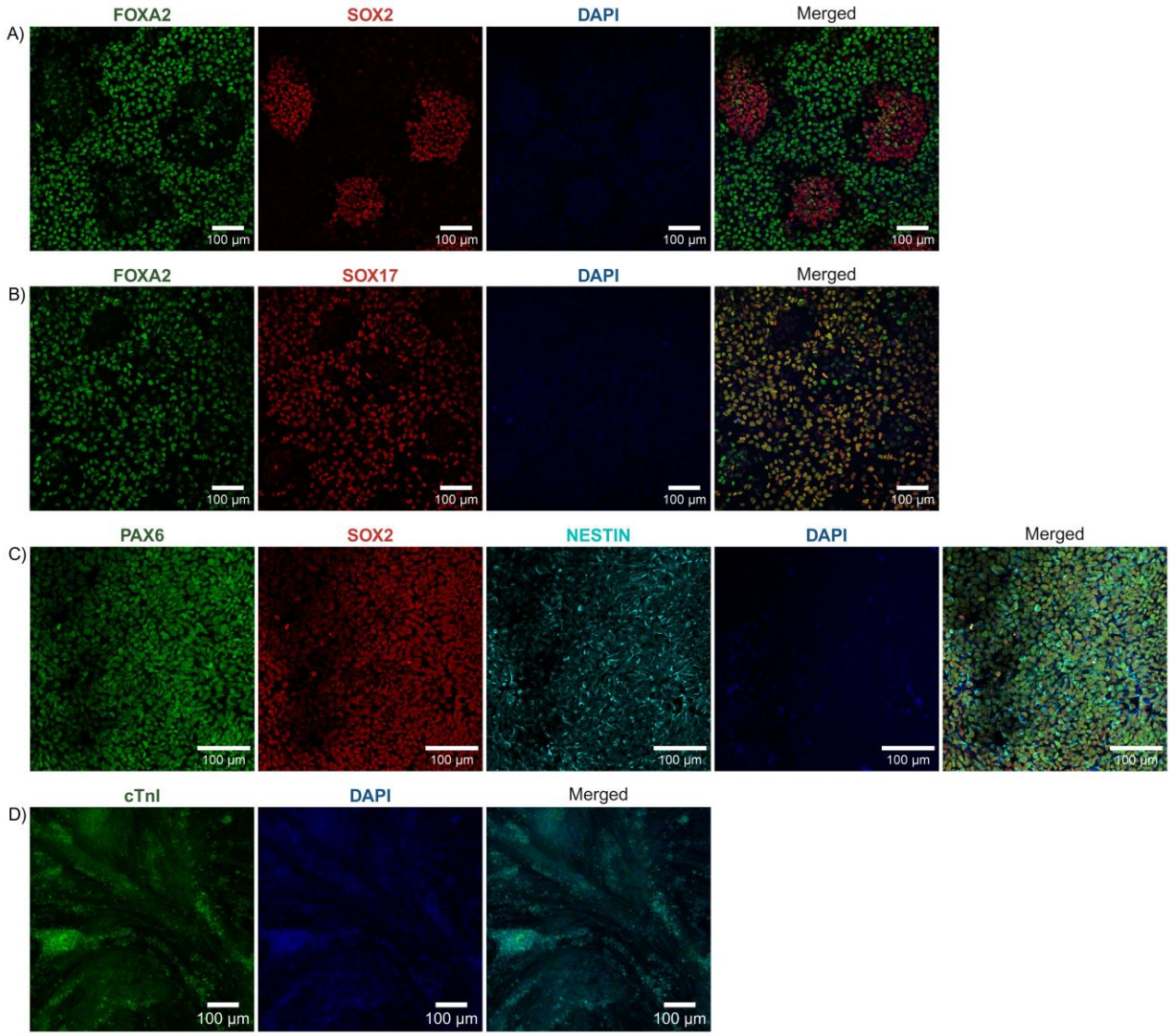

Supplementary figure 5. Single channels of the immunofluorescence analyses for the tri-lineage differentiation assay. (A) Definitive endoderm cultured with B27 (-) + 4 µM CHIR. FOXA2 (first from left, green), SOX2 (second from left, red), DAPI (third from left, blue) and merged (right) (100 µm scale bar). Zeiss LSM 880 Airyscan FAST confocal microscope. (B) Definitive endoderm cultured with B27 (-) + 3 µM CHIR. FOXA2 (first from left, green), SOX17 (second from left, red), DAPI (third from left, blue) and merged (right) (100 µm scale bar). (C) Neuroepithelium immunofluorescence analysis. PAX6 (first from left, green), SOX2 (second from left, red), NESTIN (third from left, cyan) and DAPI (fourth from left, blue) and merged (right) (100 µm scale bar). (D) Cardiomyocyte immunofluorescence analysis. cTnI (left, green), DAPI (middle, blue) and merged (right) (100 µm scale bar).

Supplementary figure 6

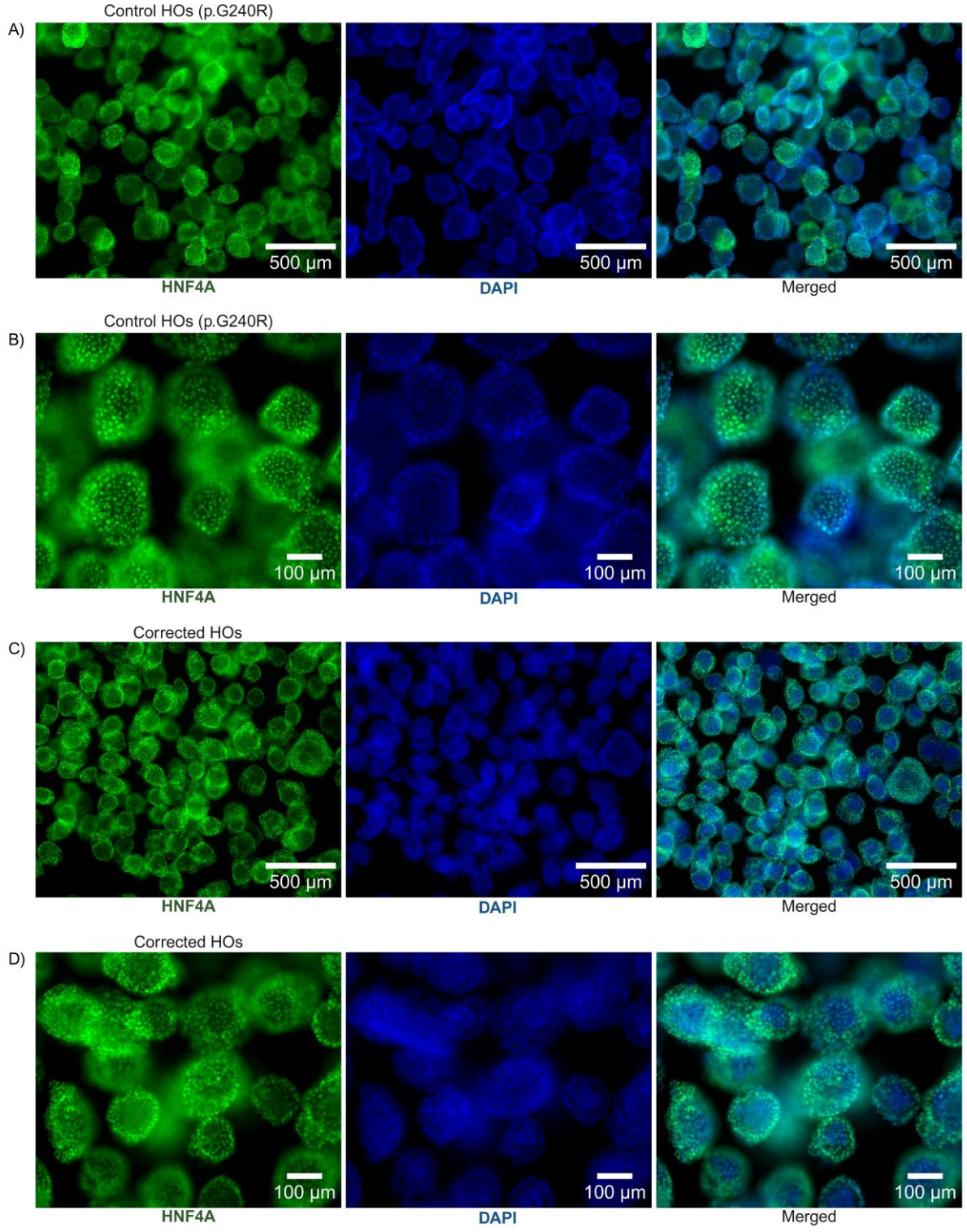

Supplementary figure 6. Single channels of the immunofluorescence analyses for HNF4A on p.G240R control and corrected HOs, at day 6. (A) p.G240R control HOs (4x magnification) (500 µm scale bar). HNF4A (left, green), DAPI (middle, blue) and merged (right). ECHO Revolve RVL-100-M. (B) p.G240R control HOs (10x magnification) (100 µm scale bar). HNF4A (left, green), DAPI (middle, blue) and merged (right). (C) Corrected HOs (4x magnification) (500 µm scale bar). HNF4A (left, green), DAPI (middle, blue) and merged (right). (D) Corrected HOs (10x magnification) (100 µm scale bar). HNF4A (left, green), DAPI (middle, blue) and merged (right).

Supplementary figure 7

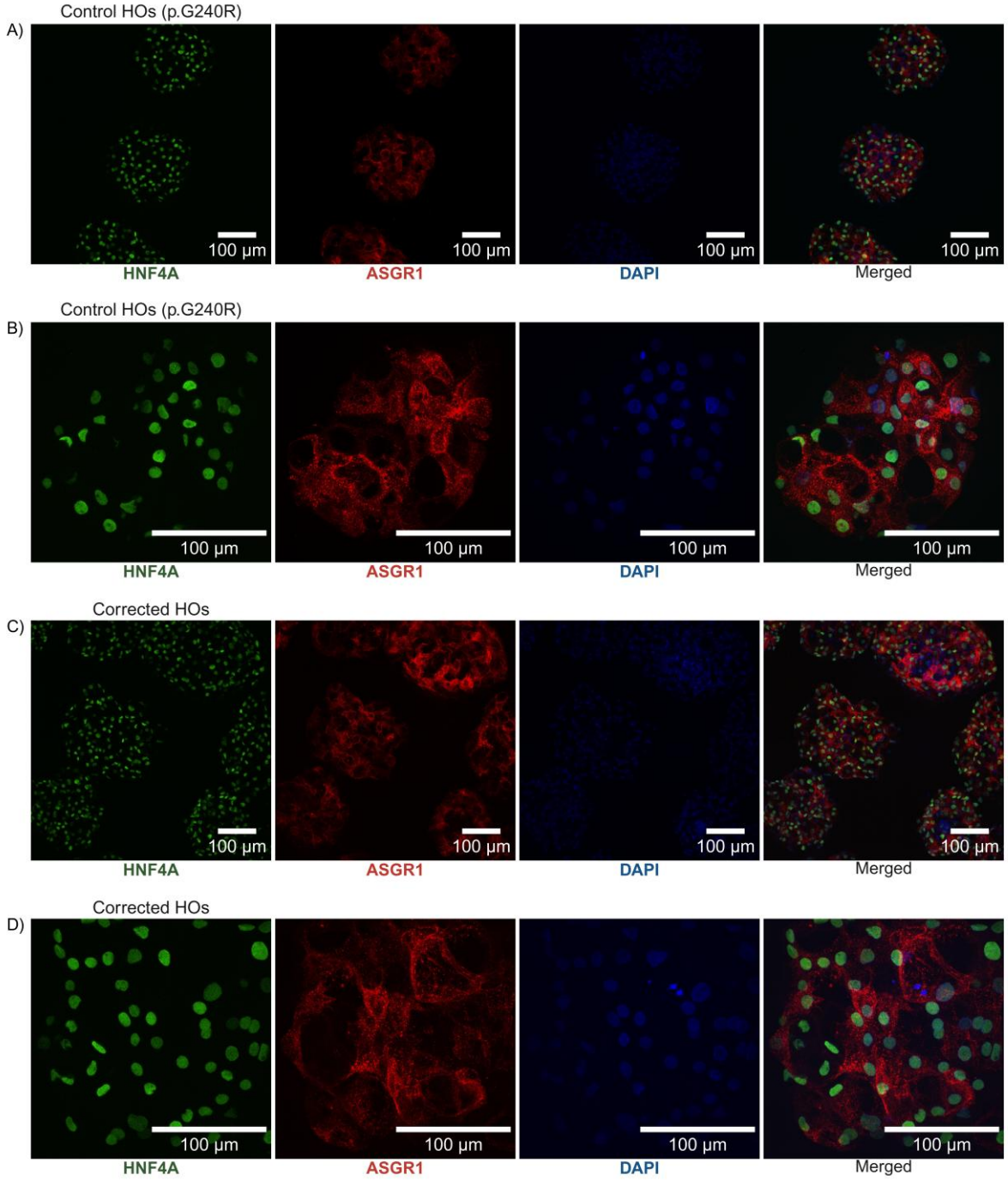

Supplementary figure 7. Single channels of the immunofluorescence analyses for ASGR1 and HNF4A markers on p.G240R control and corrected HOs, at day 19. (A) p.G240R control HOs. HNF4A (first from left, green), ASGR1 (second from left, red), DAPI (third from left, blue) and merged (right) (20x magnification) (100 µm scale bar). Andor Dragonfly Spinning Disk confocal microscope. (B) p.G240R control HOs (60x magnification) (100 µm scale bar). (C) Corrected HOs (20x magnification) (500 µm scale bar). (D) Corrected HOs (60x magnification) (100 µm scale bar).

Supplementary figure 8

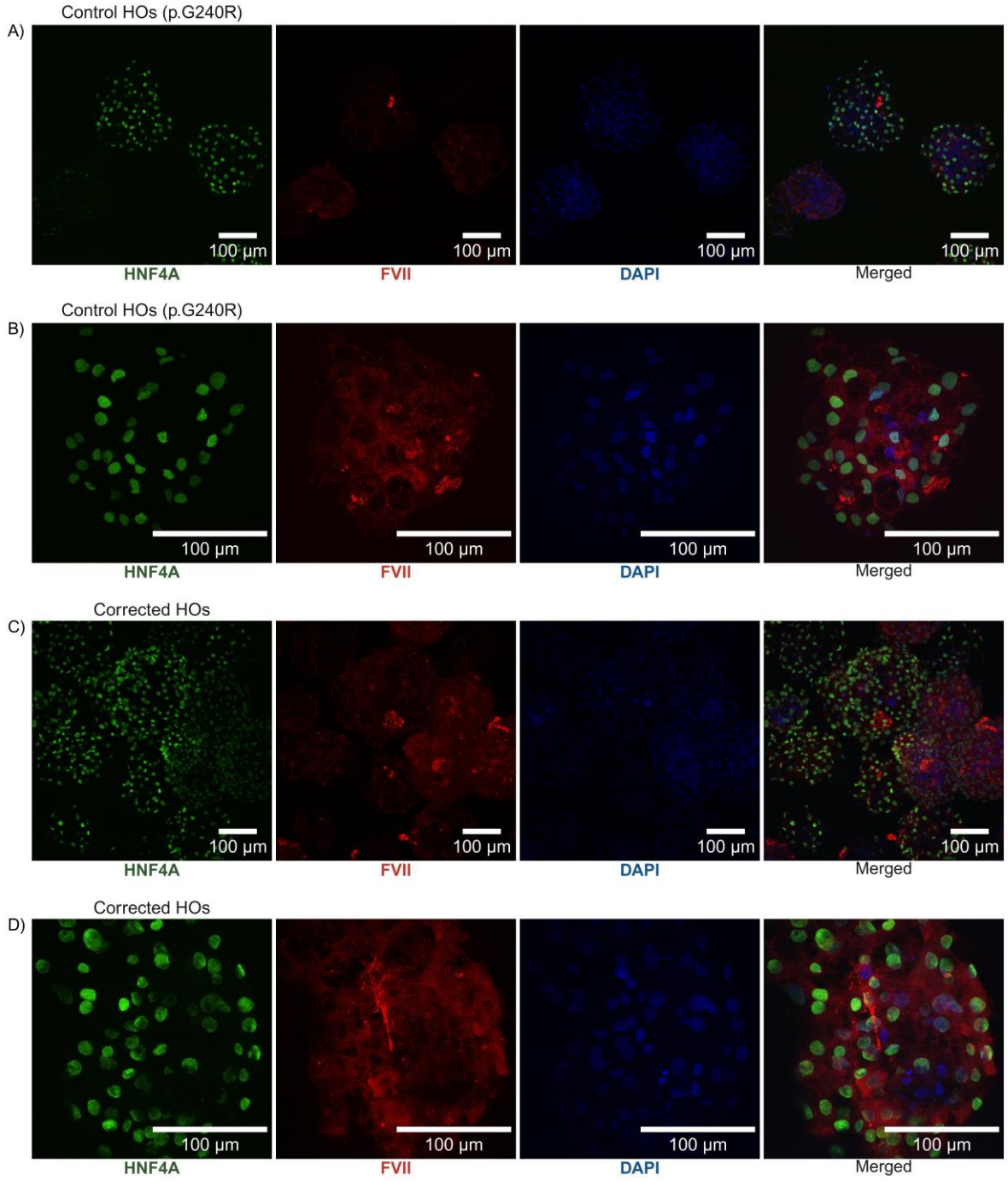

Supplementary figure 8. Single channels of the immunofluorescence analyses for FVII and HNF4A markers on p.G240R control and corrected HOs, at day 19. (A) p.G240R control HOs. HNF4A (first from left, green), FVII (second from left, red), DAPI (third from left, blue) and merged (right) (20x magnification) (100 µm scale bar). Andor Dragonfly Spinning Disk Confocal Microscope. (B) p.G240R control HOs (60x magnification) (100 µm scale bar). (C) Corrected HOs (20x magnification) (500 µm scale bar). (D) Corrected HOs (60x magnification) (100 µm scale bar).

Supplementary figure 9

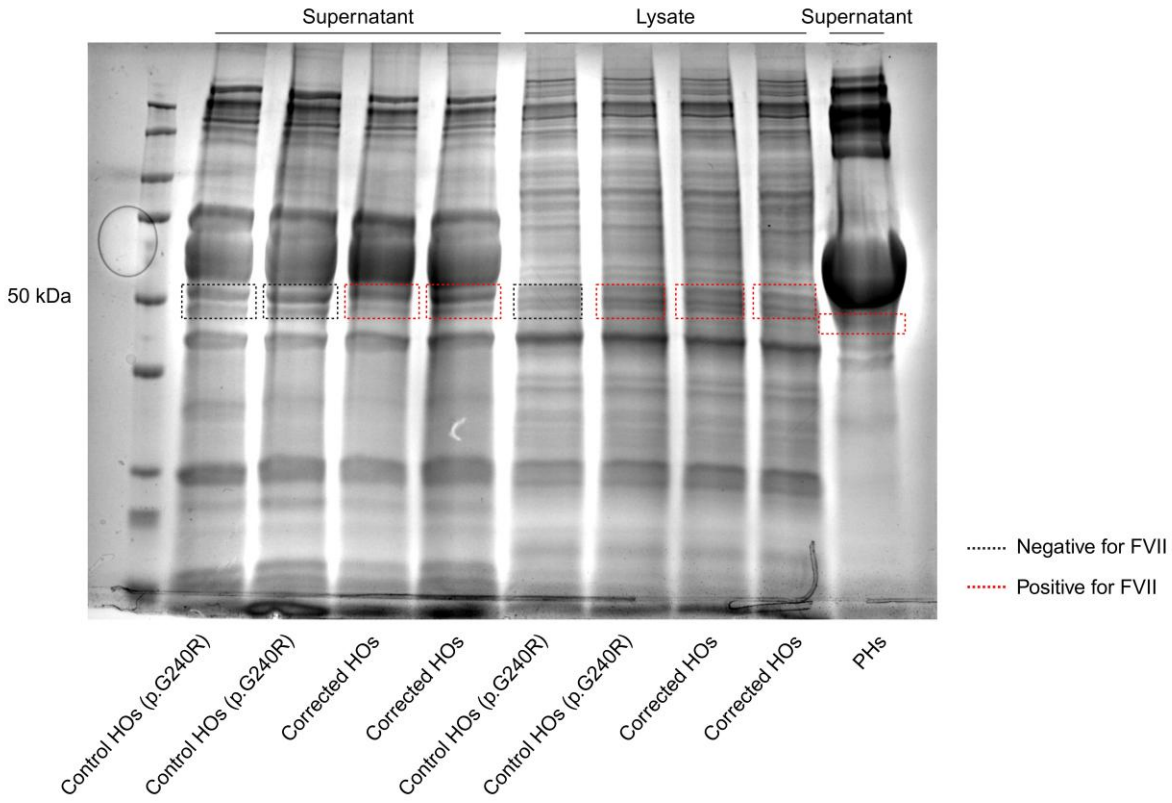

Supplementary figure 9. LC-MS analysis. SDS-PAGE of HO culture supernatants and cellular lysates. The gel samples of 40-60 kDa analyzed are indicated by black (negative for FVII) and red (positive for FVII) boxes.

Supplementary table file legends - See Excel File

Supplementary table file 1. Reagent and resource list. (A) List of primary and secondary antibodies used in this study. (B) Reagents and components. (C) Commercial assays and kits. (D) Oligonucleotide list that includes primers and TaqMan assays. (E) Software.

Supplementary table file 2. WES germline filtering and off-target prediction. (A) Results of the WES germline filtering. The silent, PAM-altering variant is highlighted in green. Variants were additionally verified using Integrative Genomics Viewer (IGV; igv.org) and marked with an asterisk (*) if visualized in the control iPSCs (c.718G>C, p.G240R). (B) Off-target sequences and sites predicted by IDT. (C) Off-target sequences and sites predicted by Benchling.

Supplementary video file legend

Supplementary video file 1. Contracting iPSC-derived cardiomyocytes. Bright-field microscopy recording of spontaneously contracting iPSC-derived cardiomyocytes at 2 weeks of differentiation, as part of the tri-lineage differentiation assay to assess pluripotency. ECHO Revolve RVL-100-M (40x magnification).

Supplementary materials and methods

Extended methods

The study was approved by the Norwegian regional committees for medical and health research ethics (REK 2018/777) and the Data Protection Officer at Oslo University Hospital (PVO #18/20935). The study was conducted in accordance with the Helsinki Declaration.

The reagent and resource list is present in the supplementary information (Supplementary information, table 1).

Generation and culturing of patient-derived iPSCs

Peripheral blood mononuclear cells (PBMCs) were isolated by Lymphoprep (STEMCELL; Vancouver, British Columbia, Canada) from blood samples collected from the FVII deficient patient, after written informed consent from the parents was obtained. The ethical approval was obtained from the data protection officer at Oslo University Hospital. The PBMCs were then reprogrammed to iPSCs by using the CytoTune-iPS 2.0 Sendai Reprogramming Kit (Invitrogen; Waltham, Massachusetts, USA), following the manufacturer's recommendations. When iPSC colonies appeared, they were picked and transferred to Geltrex LDEV-Free Reduced Growth Factor Basement Membrane Matrix (Gibco; Waltham, Massachusetts, USA)-treated 6 well plates (Thermo Fisher Scientific; Waltham, Massachusetts, USA) and cultured on. iPSCs were routinely expanded by clump passaging in 6 well plates, using 0.5 mM EDTA. The iPSCs were maintained at 37 °C, 5% CO_2 and in Essential 8 Medium (Gibco), supplemented with Penicillin-Streptomycin (10,000 U/mL) (Gibco) at 1% final concentration.

Tri-lineage assessment of pluripotency

Pluripotency of the iPSCs was investigated by direct differentiation to the three different germ layers. The iPSCs were directed to the definitive endoderm using the protocol developed by Mathapati et al., 2016[1] and Harrison et al., 2023[2], based on CHIR99021 treatment of iPSCs. To assess mesoderm differentiation, we used the protocol from Lian et al., 2013[3] to produce functional cardiomyocytes using various concentrations of CHIR99021 (4 µM – 10 µM) and 5 µM IWP 2 (Tocris). To assess ectoderm potential, we employed the method described by Chambers et al., 2009[4] and Maroof et al., 2013[5]. In short, neural epithelial cells were generated by using N-2 Supplement (100X) (Gibco), 10 µM SB 431542

(Tocris), 100 nM LDN-193189 (Selleckchem; Houston, Texas, USA) and 2 µM XAV 939 (Tocris).

Karyotyping

The iPSCs were karyotyped by KaryoStat+ Genetic Stability Assay Service (Thermo Fisher Scientific).

Genomic DNA and RNA isolation

Genomic DNA (gDNA) was isolated by using either the DNeasy Blood & Tissue Kit (Qiagen; Venlo, The Netherlands) or the Phire Animal Tissue Direct PCR Kit (Thermo Scientific), depending on the application. Total RNA was isolated by using the MagMAX-96 Total RNA Isolation Kit (Invitrogen).

Polymerase chain reaction (PCR) and reverse transcription quantitative PCR (RT-qPCR)

PCRs were performed using AmpliTaq Gold 360 Master Mix (Applied Biosystems; Waltham, Massachusetts, USA). The optimal annealing temperature and GC Enhancer amount was identified using gradient PCR. PCR products were confirmed by agarose gel electrophoresis, using a 1:5 dilution with gel loading dye (Purple (6X) (NEB; Ipswich, Massachusetts). When needed, the PCR products were purified using GeneJET PCR Purification Kit (Thermo Fisher Scientific). For reverse transcription quantitative polymerase chain reaction (RT–qPCR), total RNA was reversely transcribed to cDNA using qScript cDNA Synthesis Kit (QuantaBio; Beverly, Massachusetts, USA). Gene expression was assessed using TaqMan assays and analyzed with QuantStudio™ Software V1.3. All graphs were generated using GraphPad Prism v10.2.0.

CRISPR gene editing

Guide RNAs (gRNAs) and single-stranded oligodeoxynucleotides (ssODNs) donors were designed using the Alt-R CRISPR HDR Design Tool (IDT; Newark, New Jersey, USA) and Benchling software design tools (Benchling; San Francisco, California, USA). Donor templates consisted of symmetric homology arms of 40 bp, the corrective c.718C>G change and a protospacer adjacent motif (PAM)-altering modification. The PAM-altering

modifications were designed with Benchling software design tool as single-nucleotide, synonymous variants, to avoid re-cutting at the target locus, and further analyzed with MutationTaster2021, BDGP (https://www.fruitfly.org/seq_tools/splice.html), MobiDetails[6] and GeneBe (https://genebe.net/). The gene editing experiments were performed by nucleofection (Neon transfection system, Thermo Fisher Scientific) of ribonucleoprotein (RNP) complexes, assembled following IDT's recommendations[7]. In short, the CRISPR RNA (crRNA):transactivating crRNA (tracrRNA) duplexes were prepared by mixing the customized crRNAs and the Alt-R CRISPR-Cas9 tracrRNA ATTO 550, in equimolar concentrations. RNP complexes were generated by combining the Alt-R S.p. HiFi Cas9 Nuclease V3 with the crRNA:tracrRNA duplexes. The electroporation mixture was assembled by combining 1 µL RNP complex, 9 µL cell suspension and 2 µL Resuspension Buffer R, or Alt-R HDR Donor Oligo. 10 µL of this mixture was pipetted into the Neon Pipette Station and nucleofected at 1400 V, with 1 pulse at 20 ms pulse width. For screening of cleavage efficiency of each gRNA, gDNA was isolated after <72 hours.

Droplet digital PCR (ddPCR)

The ddPCR was performed by using customized Non-Homologous End Joining (NHEJ) Genome Edit Detection Assays (BioRad; Hercules, California, USA) and HDR Genome Edit Detection Assays (BioRad), following the manufacturers' instructions. The reactions were prepared by using the ddPCR Supermix for Probes (No dUTP) (BioRad) and 20 ng gDNA input template. The droplets were generated with the QX200 Droplet Generator (BioRad) and analyzed on a QX200 Droplet Reader (BioRad). Data analysis was performed using QX Manager Software, Standard Edition v2.1 (Bio-Rad).

Immunofluorescence and microscopy

Immunofluorescence analyses were performed following the methods described by Harrison et al., 2023[2] for the HOs and the Cell Signaling protocol (Danvers, Massachusetts, USA) for the iPSCs. Samples on µ-Slide 2 Well chambers were fixed with 4% paraformaldehyde (Thermo Fisher Scientific) for 15 minutes and blocked with 10% normal donkey serum (Abcam; Cambridge, United Kingdom), 0.3% triton X-100 (Sigma-Aldrich; Burlington, Massachusetts, USA) in Dulbecco's phosphate-buffered saline with no calcium or magnesium ($DPBS^{-/-}$). The antibodies were diluted in 10 mg/mL bovine serum albumin (Sigma-Aldrich) and 0.3% triton X-100 $DPBS^{-/-}$. Samples were mounted with ProLong Glass Antifade Mountant with NucBlue Stain (Invitrogen). HO suspensions were fixed for 30

minutes, then permeabilized and blocked with 10% normal donkey serum in 0.1% triton X-100 $DPBS^{-/-}$ for 30 minutes. The primary antibodies were directly diluted in the suspension and incubated for 1 hour at 37 °C. The secondary antibodies were mixed in 1% normal donkey serum and 0.1% triton $DPBS^{-/-}$, and incubated for 1 hour at 37 °C. A negative control immunostaining was performed using only secondary antibodies. The HOs were mounted with NucBlue Fixed Cell ReadyProbes Reagent (4',6-diamidino-2-phenylindole (DAPI)) (Invitrogen). Imaging was performed using the ECHO Revolve RVL-100-M, Zeiss LSM 880 Airyscan FAST confocal microscope and Andor Dragonfly Spinning Disk confocal microscope.

iPSCs single cell cloning

iPSCs were pre-incubated with E8 supplemented with 10 µM Y-27632 (Tocris), for 1 hour at 37 ºC, 5% CO_2. Then iPSCs were treated with StemPro Accutase (Gibco) supplemented with 10 µM Y-27632, for <10 minutes at 37 ºC, 5% CO_2. The iPSCs were resuspended with complete StemFlex Medium (Gibco), supplemented with 10 µM Y-27632, and filtered through a 20 µm strainer (SEED Biosciences; Epalinges, Switzerland) twice. Cells were counted with trypan blue exclusion, pelleted at 200xg for 5 minutes and resuspended at 150’000 cells/mL in StemFlex-Y-27632. 15 µL of the cell suspension was moved into the DispenMe (SEED Biosciences) vial and gently resuspended. Following the manufacturer’s instructions, the cell suspension was loaded on the Dispencell (SEED Biosciences) cell seeding device and dispensed at 1 cell/well, into Vitronectin (VTN-N) Recombinant Human Protein, Truncated (Thermo Fisher Scientific)-coated 96 well plates, which had been pre-warmed and filled with 100 µL/well StemFlex-Y-27632. Wells in which more than one cell (multiple single cell events, doublets or aggregates) was dispensed, or where the detection signal was ambiguous or uncertain, were excluded. An optimal particle size was defined by an impedance range of ≥400 to ≤3,000 ohm. After <48 hours, fresh 150 µL StemFlex were added to dilute the Y-27632. After 48 hours, 150 µL were removed from each well and replaced with fresh StemFlex. After that, iPSCs were expanded with regular medium changes.

Sanger Sequencing and Whole Exome Sequencing (WES)

Sanger sequencing, Illumina WES analyses at 30x coverage (Clinical Research Exome - CRE V4) and 100x coverage (INVIEW Human Exome) and downstream bioinformatic analysis were performed by Eurofins Genomics (Ebersberg, Germany).

Hepatic organoid differentiation

Hepatic organoids (HOs) were generated using the protocol developed by Harrison et al.[2],. In short, iPSCs were seeded as single cells in 125 mL PC Erlenmeyer Shaker Flasks (VWR; Radnor, Pennsylvania, USA), at a concentration of $2.5 \cdot 10^5$ cells/mL in 20 mL E8, supplemented with CultureCEPT Supplement (Gibco). After 16 hours (day 0), the HOs were cultured with RPMI-B-27 Supplement (Gibco), minus insulin, supplemented with 3.8 µM CHIR99021. After 24 hours (day 1), the medium was replaced with RPMI-B-27 Supplement, minus insulin, without CHIR99021. The HOs were then cultured with SR-DMSO from day 2 until day 6, and with L-15 medium from day 7 until day 19. On day 19, the HOs were washed twice with 20 mL L-15 base (Sigma-Aldrich) and then incubated with serum-free L-15 medium, formulated as described by Harrison et al., 2023[2] but devoid of fetal bovine serum (Biowest; Bradenton, Florida, USA) and supplemented with 5 µg/mL Vitamin K_1. Both HOs and the cell supernatant were collected on day 21 for the downstream analyses, after 2 days in serum-free conditions.

Protein determination and activity assay

Supernatants were harvested from HO suspensions by centrifugation for 5 minutes at 300xg without brake and collected in 2 mL tubes. The supernatants were then centrifuged at 4 ºC, 18'118xg, for 15 minutes, and stored at -80 ºC. Protein levels (FVII:Ag) were analyzed by U-PLEX Human Factor VII Assay (Mesoscale Diagnostic; Rockville, Maryland, USA), following the manufacturer's instructions. FVII activity (FVII:C) was measured using the BIOPHEN FVII assay kit (Aniara; West Chester Township, Ohio, USA). Factor X (Abcam), albumin (Nordic Biosite; Täby, Stockholm) and α-1 Antitrypsin (A1AT) (Abcam) antigens were measured by enzyme-linked immunosorbent assay (ELISA). Thrombin generation was assessed using the calibrated automated thrombogram (CAT) (Diagnostica Stago, Asnières sur Seine, France), as described by Harrison et al.[2]. 50 µL sample was mixed with 30 µL of FVII-deficient plasma (HemosIL, Instrumentation Laboratory Company, Bedford, MA, USA) and 20 µL of either 1 pM (PPP reagent low) or 5 pM tissue factor (TF) (PPP reagent). After 10 minutes incubation at 37 °C, the thrombin generation was initiated by adding 20 µL of fluorogenic substrate in a buffer containing calcium chloride (FluCa). All the reagents were provided by Diagnostica Stago. The fluorescence was measured kinetically at 37 °C for up to 80 minutes and the results were analyzed in the thrombinoscope software. Controls included L-15 medium as negative control, PHs and pooled normal plasma (PNP) as positive controls. Cell pellets were obtained by centrifugation of 5 mL of HO suspension, the supernatant was removed and the pellet resuspended with 1 mL T-PER Tissue Protein

Extraction Reagent (Thermo Fisher Scientific), supplemented with Halt Protease and Phosphatase Inhibitor Cocktail (100X) (Thermo Fisher Scientific), and homogenized with BD Microlance 18 G needle (Becton Dickinson; Franklin Lakes, New Jersey, USA). Sample homogenates were centrifuged at 8'000xg for 10 minutes, at 4 ºC, to obtain a clear fraction and stored at -80 ºC. The total cellular protein was quantified with Pierce BCA Protein Assay Kits (VWR). As a positive control, Human Plateable Hepatocytes, Uptake Qualified (Gibco) were cultured as a dense population of $1 \cdot 10^6$ cells/mL, in 2 mL maintenance medium (Gibco), following the manufacturer's recommendations. Samples were collected after 48 hours in maintenance medium and processed as above to generate lysates. As additional positive reference for the FVII chromogenic activity assay, HOs generated from a wild-type, healthy and unedited iPSC line (AG27) were used[2].

Liquid chromatography-mass spectrometry (LC-MS) analysis

Proteins from culture supernatants (concentrated) and cellular lysates were separated by SDS-PAGE and stained with Coomassie Blue (Thermo Fisher Scientific). Gel bands of size 40-60 kDa were excised and subjected to in-gel digestion using trypsin, after which the resulting proteolytic fragments were desalted using 10 µL STAGE-tips (Affinisep; Le Houlme, France). The samples were analyzed by LC-MS using a timsTOF Pro (Bruker Daltonik; Bremen, Germany) which was coupled online to a nanoElute nanoflow liquid chromatography system (Bruker Daltonik) via a CaptiveSpray nanoelectrospray ion source. The dried peptides were dissolved in 4 µL 0.1% formic acid and 2 µL of sample was injected. The peptides were separated on a reversed phase Aurora Elite CSI UHPLC column (C18, 15 cm x 75 µm, 1.7 µm) (IonOpticks; Fitzroy, VIC, Australia). Mobile phase A contained water with 0.1% formic acid, and acetonitrile with 0.1% formic acid was used as mobile phase B. The peptides were separated by a gradient from 0-35% mobile phase B over 30 min at a flow rate of 200 nL/min at a column temperature of 50°C. MS acquisition was performed in DDA-PASEF mode. The LC-MS data were searched against the UniProt database of Homo sapiens (20,429 entries) using Mascot version 3.0 (Matrix Science; London, UK). The following parameters were used: digestion enzyme, trypsin; maximum missed cleavage, 1; fragment ion mass error tolerance, 0.03 Da; parent ion error tolerance, 15 ppm. Oxidation of methionine, propionamidylation of cysteine, and acetylation of the protein N-terminus were specified as variable modifications. Scaffold version 5.1.2 (Proteome Software Inc.; Portland, OR, USA) was used to validate MS/MS based peptide and protein identifications. A false-discovery rate of 1% of the peptide threshold was applied to the datasets.

Statistical analyses

The statistical analyses were performed with GraphPad Prism 10.2.0. The data were generated from three independent experiments consisting of two biological replicates for the HOs and one for the PHs and are expressed as mean and standard deviation. The normal distribution of values was assessed by Shapiro-Wilk test. For the comparison among two groups the statistical significance was determined by unpaired Student's t-test. A probability value of $p<0.05$ was considered statistically significant, with * $p<0.05$, ** $p<0.01$, *** $p<0.001$ and **** $p<0.0001$.

References to supplementary data

1. Mathapati S, Siller R, Impellizzeri AAR, et al. Small-molecule-directed hepatocyte-like cell differentiation of human pluripotent stem cells. Curr Protoc Stem Cell Biol 2016;2016(1):1G.6.1-1G.6.18.

2. Harrison SP, Siller R, Tanaka Y, et al. Scalable production of tissue-like vascularized liver organoids from human PSCs. Exp Mol Med 2023;55(9):2005–2024.

3. Lian X, Zhang J, Azarin SM, et al. Directed cardiomyocyte differentiation from human pluripotent stem cells by modulating Wnt/β-catenin signaling under fully defined conditions. Nat Protoc 2013;8(1):162–175.

4. Chambers SM, Fasano CA, Papapetrou EP, Tomishima M, Sadelain M, Studer L. Highly efficient neural conversion of human ES and iPS cells by dual inhibition of SMAD signaling. Nat Biotechnol 2009;27(3):275–280.

5. Maroof AM, Keros S, Tyson JA, et al. Directed differentiation and functional maturation of cortical interneurons from human embryonic stem cells. Cell Stem Cell 2013;12(5):559–572.

6. Baux D, Van Goethem C, Ardouin O, et al. MobiDetails: online DNA variants interpretation. Eur J Hum Genet 2021;29(2):356–360.

7. Kenny Moore C, Martin J, William S. Electroporation of human pluripotent or embryonic stem cells with CRISPR reagents Ribonucleoprotein delivery using the Alt-R ® CRISPR-Cas9 System for homology-directed repair or other genome editing applications. 2017; Coralville, IA. Integrated DNA Technologies.;1–5. www.idtdna.com/CRISPR-Cas9.